

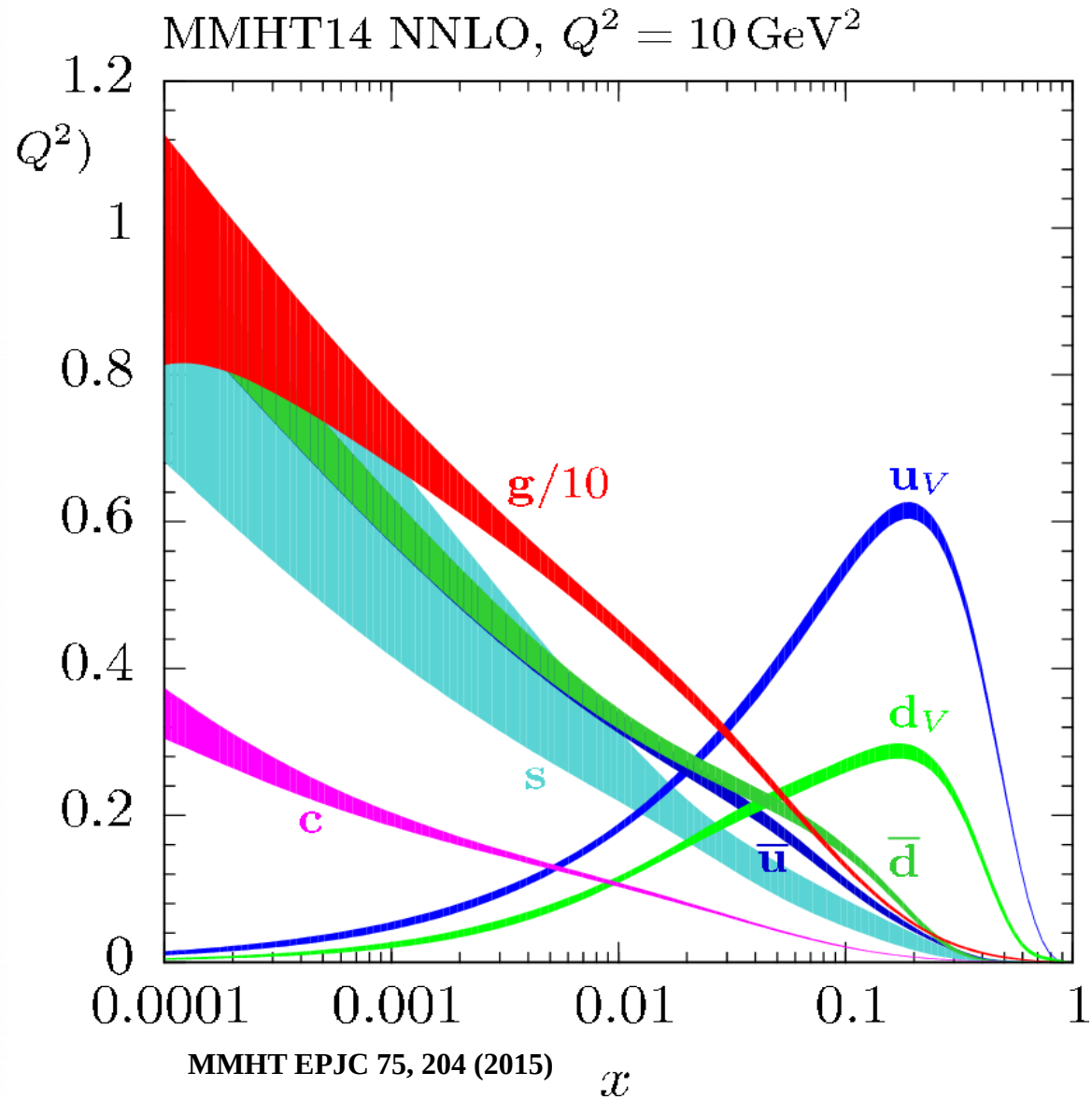
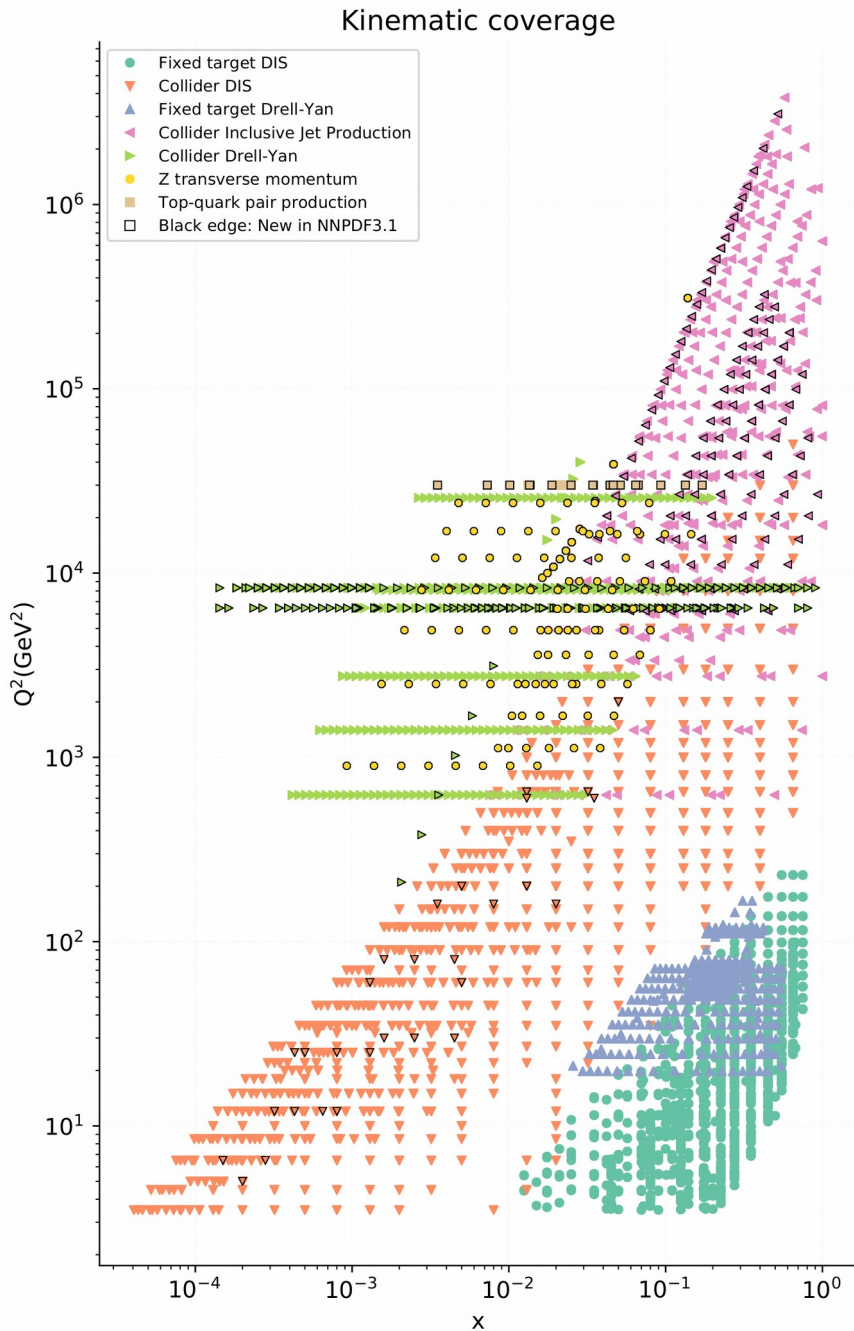
PDFs for the LHC

S.Alekhin (*Univ. of Hamburg & IHEP Protvino*)

sa, Blümlein, Moch, Plačakytė PRD 96, 014011 (2017)
sa, Blümlein, Moch PLB 777, 134 (2018)
sa, Blümlein, Moch EPJC 78, 477 (2018)
sa, Kulagin, Blümlein, Moch, Petti hep-ph/1808.06871
sa, Blümlein, Moch hep-ph/1808.08404
sa, Blümlein, Moch hep-ph/1909.03533

LFC19, Trento, 10 Sep 2019

Global PDF fits



Various processes provide constraints on various PDFs' combinations

ABM PDF fit framework

QCD evolution

massless NNLO, massive NLO OMEs
(*OPENQCDRAD*)

3-flavour PDFs

5-flavour PDFs

DIS inclusive

NNLO
(*OPENQCDRAD*)

Power corr.
(TMC+high-twist)

DIS heavy quark

NNLO(approx.)
(*OPENQCDRAD*)

Drell-Yan (W,Z, γ)

NNLO
(*FEWZ-grids*)

t-quark

(*Hathor, fasttop*)

Data used and fit quality

Experiment	Process	Reference	NDP	χ^2
<i>DIS</i>				
HERA I + II	$e^\pm p \rightarrow e^\pm X$	[4]	1168	1510
	$e^\pm p \rightarrow \overset{(-)}{\nu} X$			
BCDMS	$\mu^+ p \rightarrow \mu^+ X$	[61]	351	411
NMC	$\mu^+ p \rightarrow \mu^+ X$	[60]	245	343
SLAC-49a	$e^- p \rightarrow e^- X$	[54,62]	38	59
SLAC-49b	$e^- p \rightarrow e^- X$	[54,62]	154	171
SLAC-87	$e^- p \rightarrow e^- X$	[54,62]	109	103
SLAC-89b	$e^- p \rightarrow e^- X$	[56,62]	90	79
<i>DIS heavy-quark production</i>				
HERA I + II	$e^\pm p \rightarrow e^\pm cX$	[63]	52	62
H1	$e^\pm p \rightarrow e^\pm bX$	[15]	12	5
ZEUS	$e^\pm p \rightarrow e^\pm bX$	[16]	17	16
CCFR	$\overset{(-)}{\nu} N \rightarrow \mu^\pm cX$	[64]	89	62
CHORUS	$\nu N \rightarrow \mu^+ cX$	[18]	6	7.6
NOMAD	$\nu N \rightarrow \mu^+ cX$	[17]	48	59
NuTeV	$\overset{(-)}{\nu} N \rightarrow \mu^\pm cX$	[64]	89	49
<i>DY</i>				
FNAL-605	$pCu \rightarrow \mu^+ \mu^- X$	[68]	119	165
FNAL-866	$pp \rightarrow \mu^+ \mu^- X$	[69]	39	53
	$pD \rightarrow \mu^+ \mu^- X$			
<i>Top-quark production</i>				
ATLAS, CMS	$pp \rightarrow tqX$	[27–32]	10	2.3
CDF&DØ	$\bar{p}p \rightarrow tbX$	[53]	2	1.1
	$\bar{p}p \rightarrow tqX$			
ATLAS, CMS	$pp \rightarrow t\bar{t}X$	[33–52]	23	13
CDF&DØ	$\bar{p}p \rightarrow t\bar{t}X$	[53]	1	0.2

DY data in the ABMP16 fit

Experiment	ATLAS		CMS		DØ		LHCb			
\sqrt{s} (TeV)	7	13	7	8	1.96		7	8		
Final states	$W^+ \rightarrow l^+ \nu$ $W^- \rightarrow l^- \nu$ $Z \rightarrow l^+ l^-$	$W^+ \rightarrow l^+ \nu$ $W^- \rightarrow l^- \nu$ $Z \rightarrow l^+ l^-$	$W^+ \rightarrow \mu^+ \nu$ $W^- \rightarrow \mu^- \nu$ (asym)	$W^+ \rightarrow \mu^+ \nu$ $W^- \rightarrow \mu^- \nu$	$W^+ \rightarrow \mu^+ \nu$ $W^- \rightarrow \mu^- \nu$ (asym)	$W^+ \rightarrow e^+ \nu$ $W^- \rightarrow e^- \nu$ (asym)	$W^+ \rightarrow \mu^+ \nu$ $W^- \rightarrow \mu^- \nu$ $Z \rightarrow \mu^+ \mu^-$	$Z \rightarrow e^+ e^-$	$W^+ \rightarrow \mu^+ \nu$ $W^- \rightarrow \mu^- \nu$ $Z \rightarrow \mu^+ \mu^-$	
Cut on the lepton P_T	$P_T^l > 20$ GeV	$P_T^e > 25$ GeV	$P_T^\mu > 25$ GeV	$P_T^\mu > 25$ GeV	$P_T^\mu > 25$ GeV	$P_T^e > 25$ GeV	$P_T^\mu > 20$ GeV	$P_T^e > 20$ GeV	$P_T^\mu > 20$ GeV	
Luminosity (1/fb)	0.035	0.081	4.7	18.8	7.3	9.7	1	2	2.9	
NDP	30	6	11	22	10	13	31(33) ^a	17	32(34)	
	ABMP16	31.0	9.2	22.4	16.5	17.6	19.0	45.1(54.4)	21.7	40.0(59.2)
	CJ15	–	–	–	–	20	29	–	–	–
	CT14	42	–	– ^b	–	–	34.7	–	–	–
	HERAFitter	–	–	–	–	13	19	–	–	–
	MMHT16	39 ^c	–	–	21	21 ^c	26	(43)	29	(59)
	NNPDF3.1	29	–	19	–	16	35	(59)	19	(47)

^a The values of NDP and χ^2 correspond to the unfiltered samples.

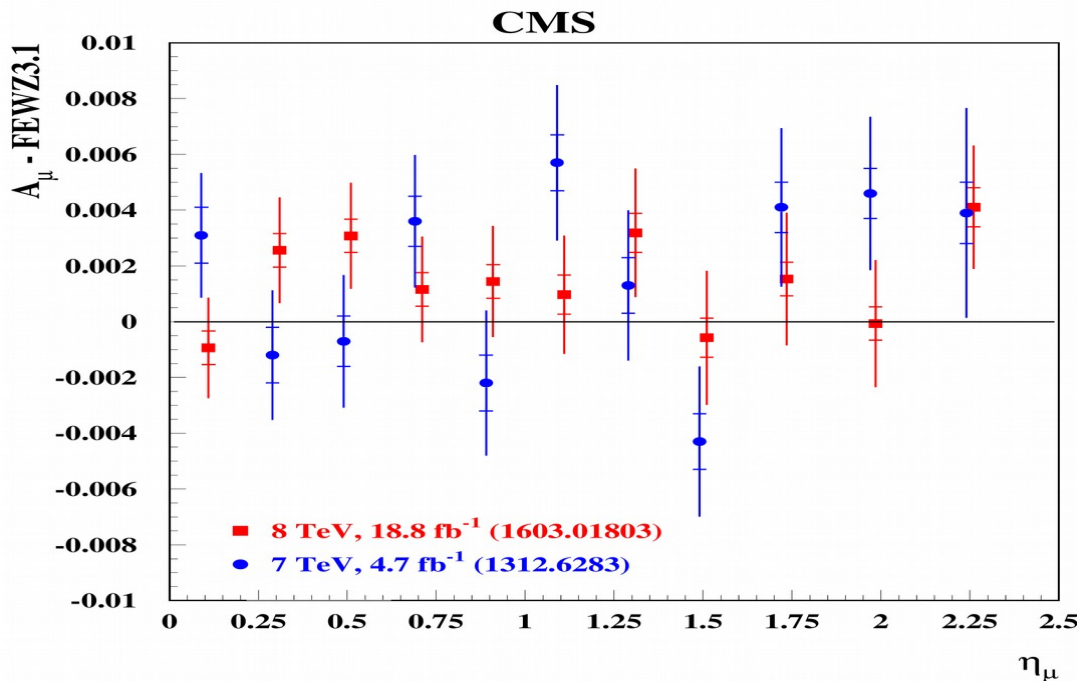
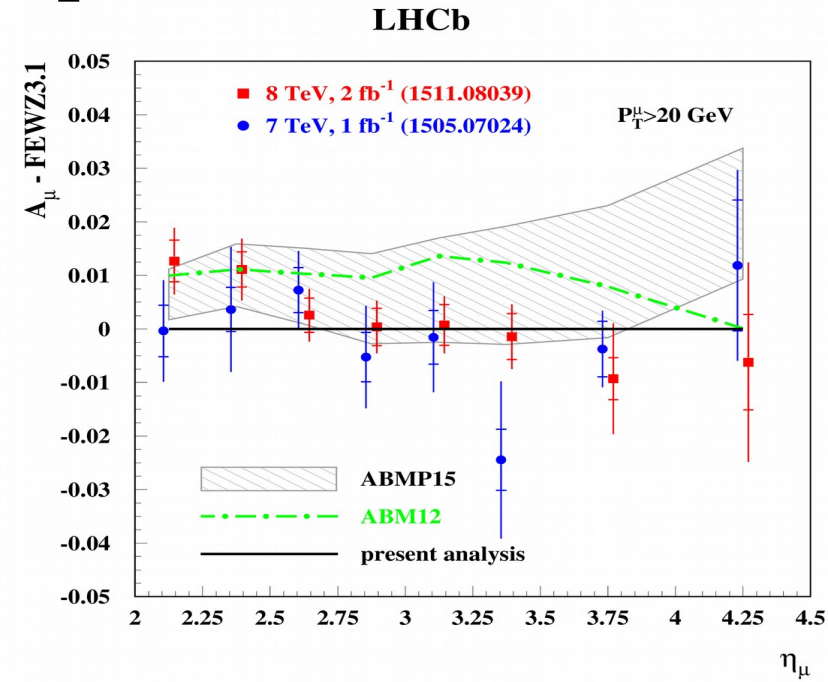
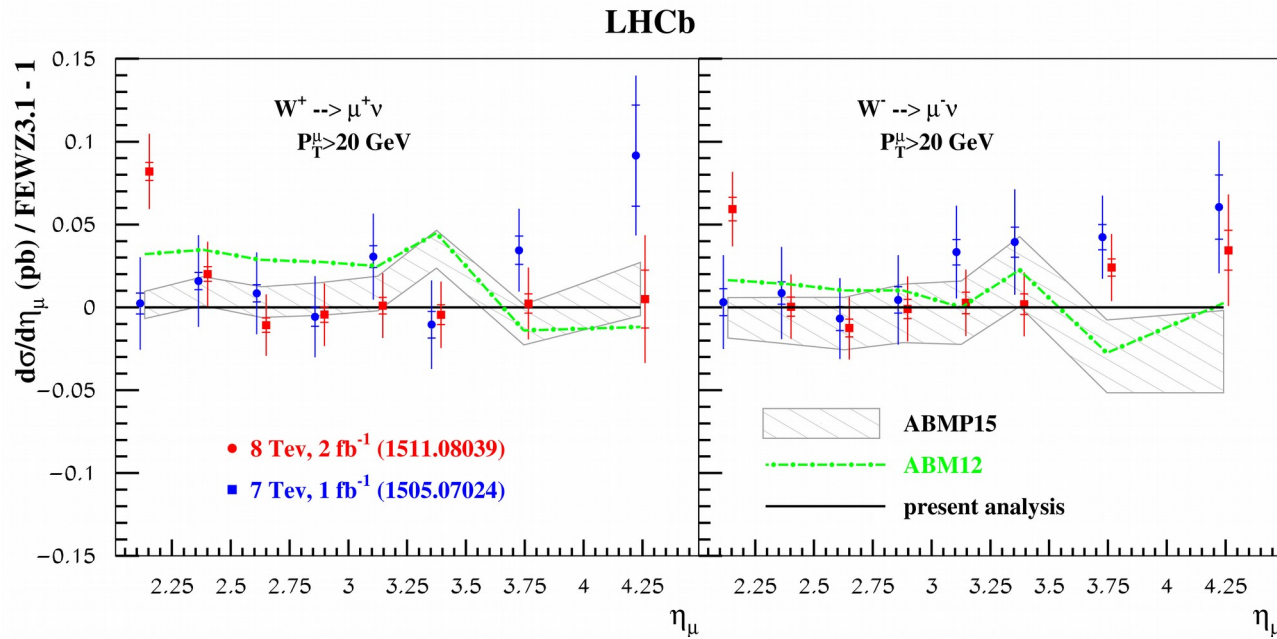
^b For the statistically less significant data with the cut of $P_T^\mu > 35$ GeV the value of $\chi^2 = 12.1$ was obtained.

^c The value obtained in MMHT14 fit.

Experiment	NDP	χ^2 after the data sets excuded				
		–	ATLAS	CMS	DØ	LHCb
ATLAS	36	37.7	–	37.0	38.3	39.6
CMS	33	26.6	25.6	–	26.0	23.5
DØ	23	48.5	48.1	47.7	–	44.2
LHCb	80	98.2	100.2	97.4	78.8	–

- Good overall agreement in NNLO with some tension between DØ and LHCb data

Most recent DY inputs



Filtering of the LHCb data has been performed:

- a bump at 7 TeV and $Y=3.275$ (not confirmed by the LHCb data at 8 TeV)
- and excess at 8 TeV and $Y=2.125$ (not confirmed by the CMS data at 8 TeV)

The CMS data at 8 TeV are much smoother than the ones at 7 TeV:
 $\chi^2=17/22$ versus $22/11$

Impact of the W-, Z-data

In the forward region $x_2 \gg x_1$

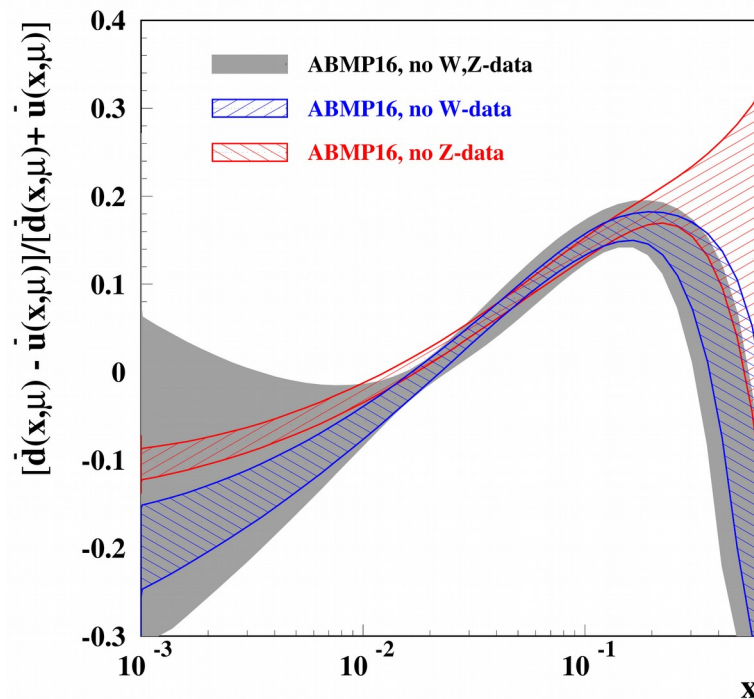
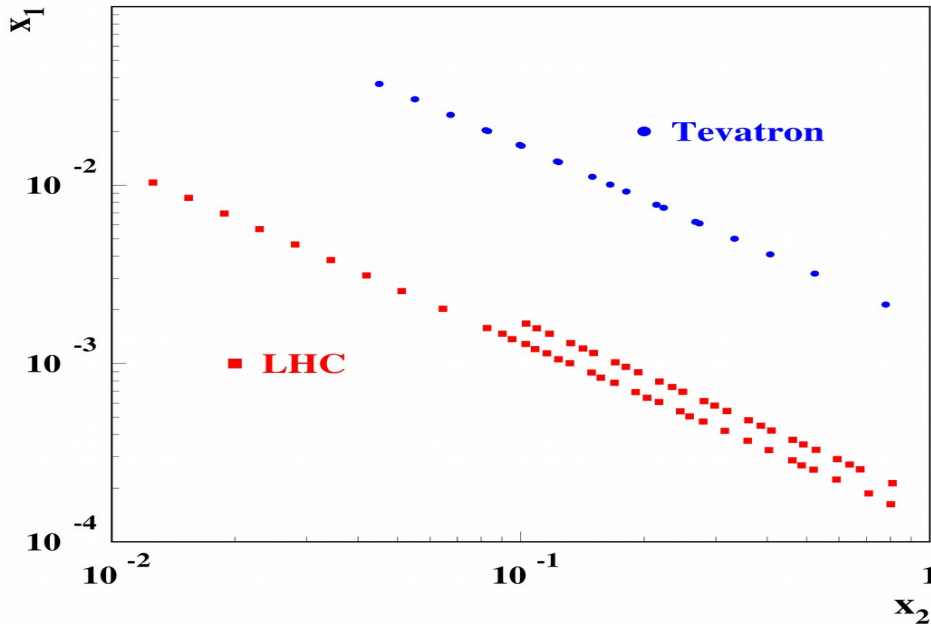
$$\sigma(W^+) \sim u(x_2) \bar{d}(x_1)$$

$$\sigma(W^-) \sim d(x_2) \bar{u}(x_1)$$

$$\sigma(Z) \sim Q_u^2 u(x_2) \bar{u}(x_1) + Q_d^2 d(x_2) \bar{d}(x_1)$$

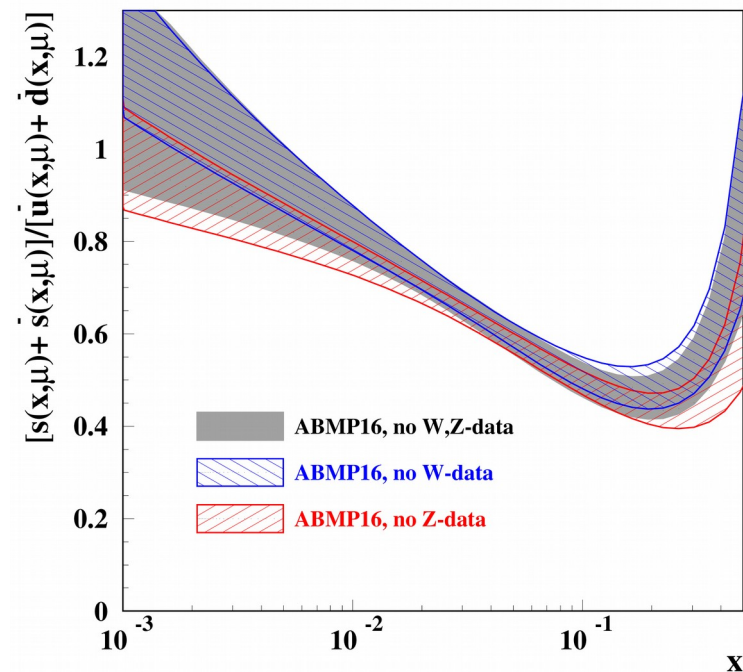
$$\sigma(\text{DIS}) \sim q_u^2 u(x_2) + q_d^2 d(x_2)$$

Forward W&Z production probes small/large x and is complementary to the DIS \Rightarrow good quark disentangling



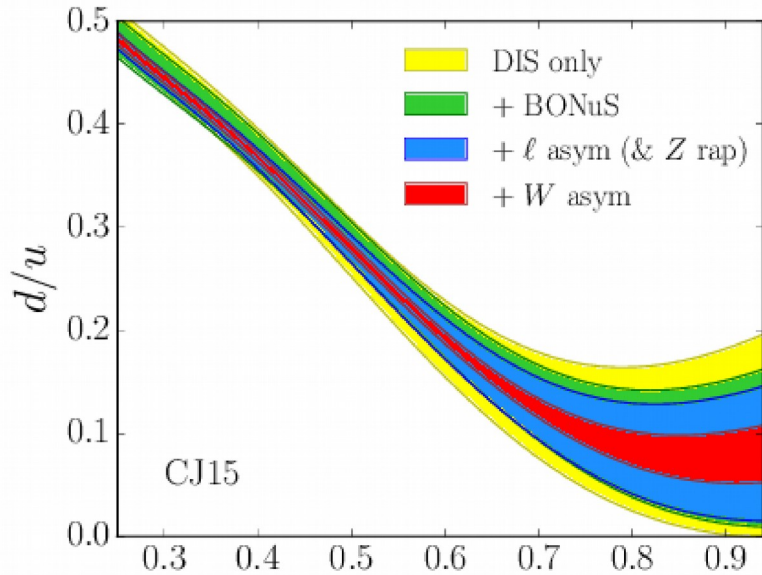
Negative small- x sea isospin asymmetry

$\mu=3 \text{ GeV}, N_f=3$

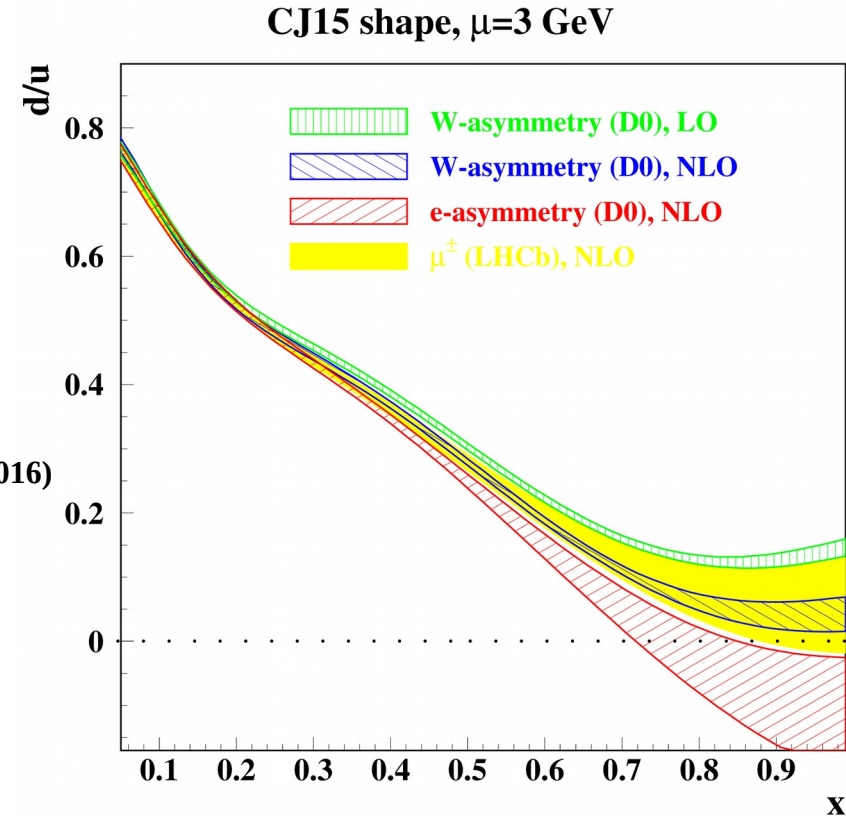


No small- x strange sea suppression

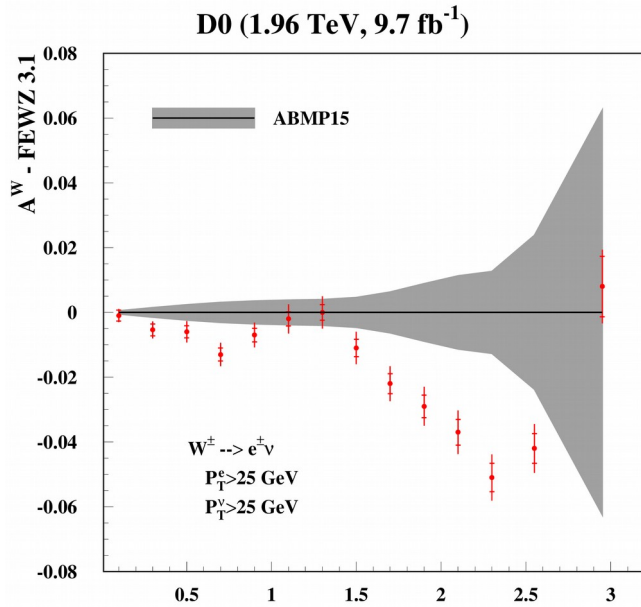
d/u at large x



Accardi, Brady, Melnitchouk, Owens, Sato PRD 93, 114017 (2016)



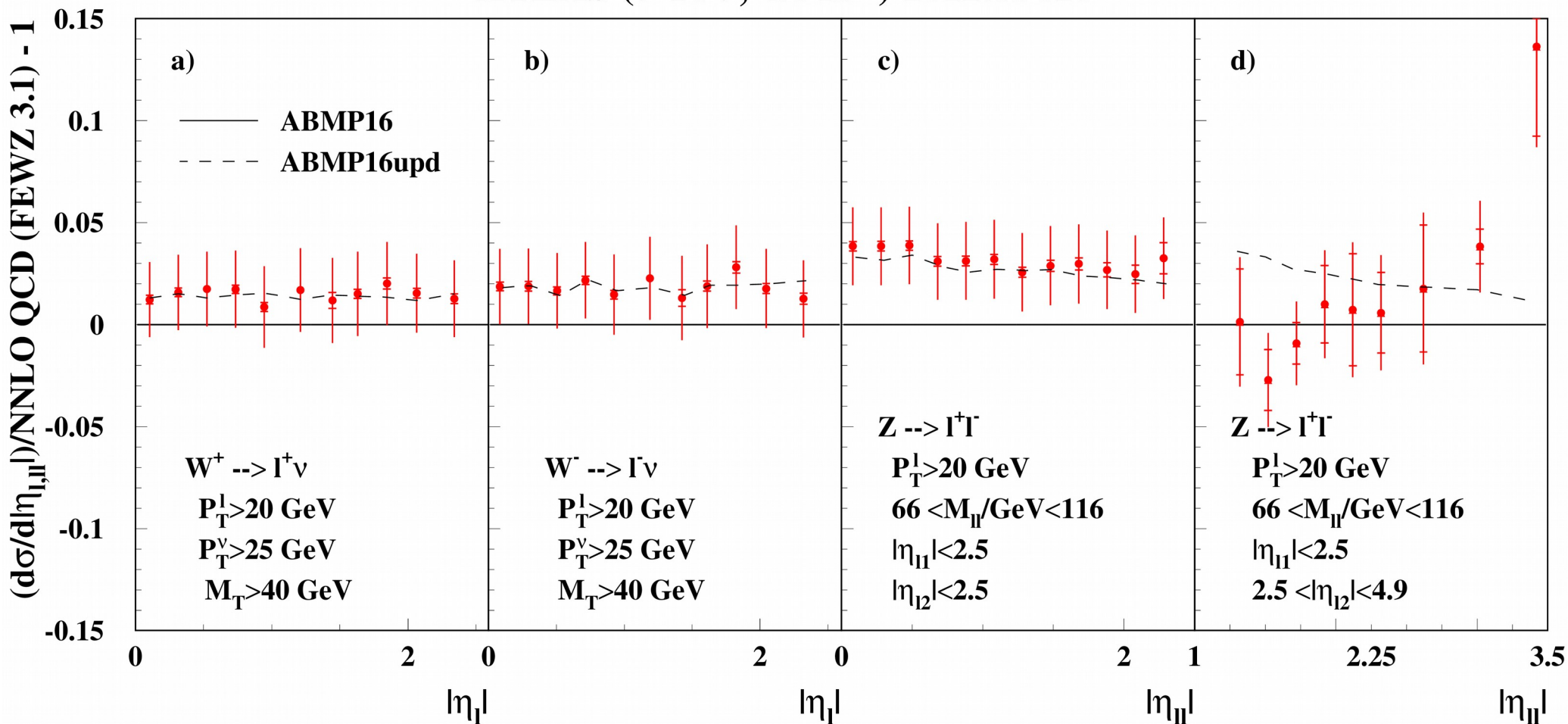
- Account of the NNLO corrections moves large-x d/u downwards
- e-asymmetry data prefer lower d/u
- d/u consistent with 0 at $x \rightarrow 1$



W-asymmetry data go lower than predictions based on the e-asymmetry: data selection is important

Recent W and Z 7-TeV ATLAS data

ATLAS (7 TeV, 4.6 fb⁻¹) 1612.03016



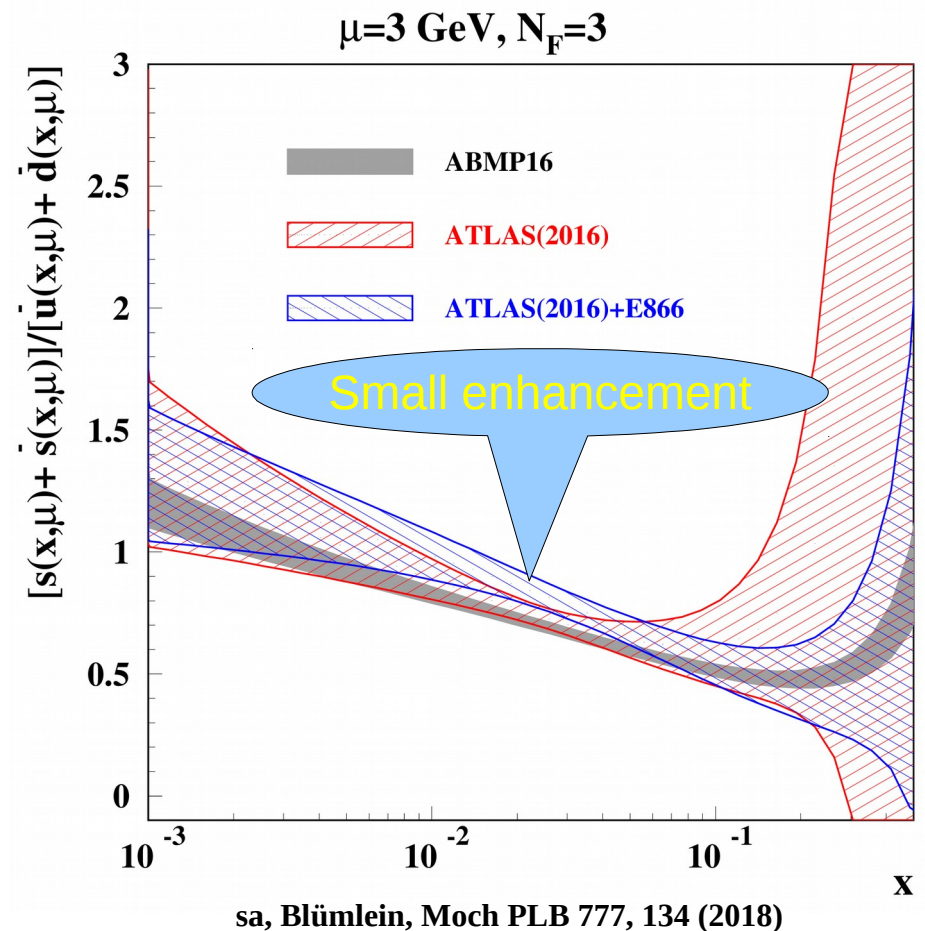
Data are well accommodated in general; forward Z-boson data have particular trend, however, χ^2 is also not bad due to large errors, 68/61 for the whole sample

Impact of ATLAS data on strangeness

	$\kappa_s(\mu^2=20 \text{ GeV}^2)$
HERA+ATLAS	0.81(18)
HERA+ATLAS+E866	0.72(8)
ABMP16(incl. NOMAD)	0.66(3)

κ_s is integral strange sea suppression factor:

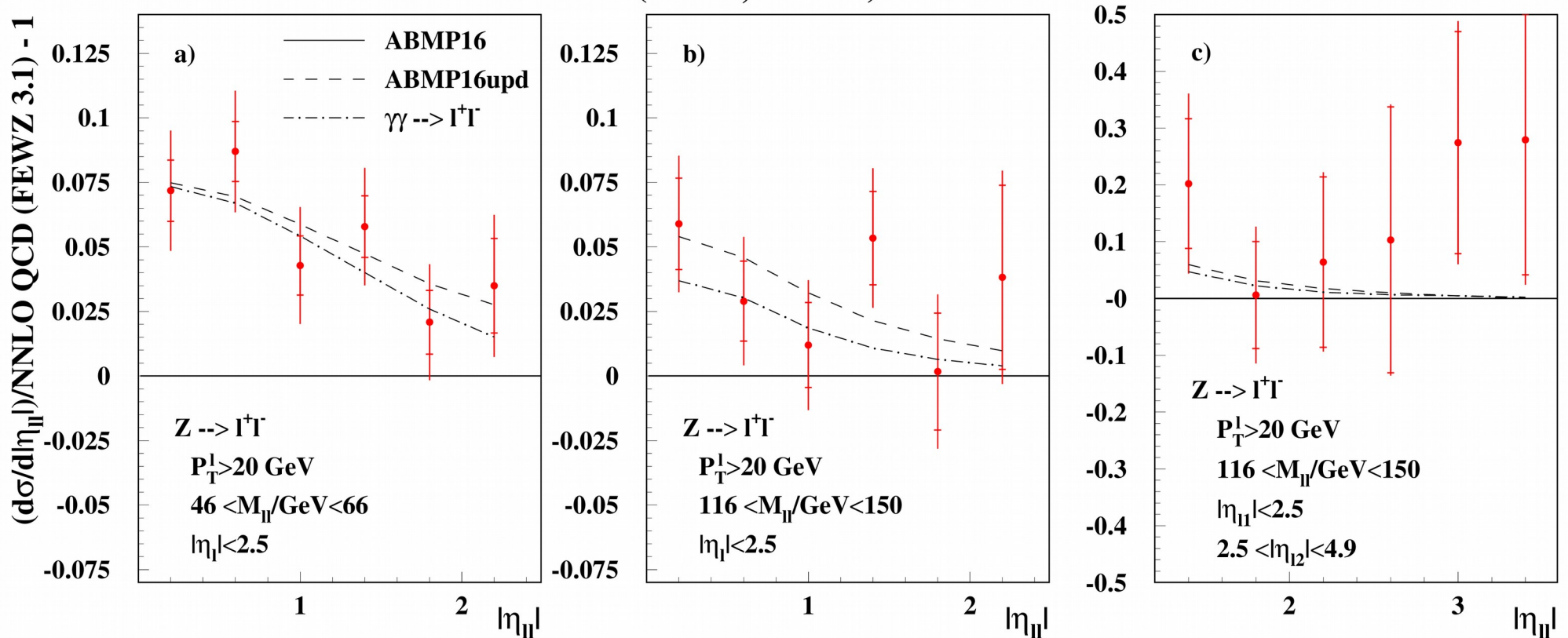
$$\kappa_s(\mu^2) = \frac{\int_0^1 x[s(x, \mu^2) + \bar{s}(x, \mu^2)]dx}{\int_0^1 x[\bar{u}(x, \mu^2) + \bar{d}(x, \mu^2)]dx},$$



- ATLAS data provide a constraint on small-x sea quarks; at moderate x additional constraint is needed, comes from fixed-target DY (FNAL-E866)
- The E866 data are consistent with the ATLAS(2016) central data: $\chi^2/\text{NDP}=48/39$ and $40/34$, respectively
- The strangeness is in a broad agreement with the one extracted from the dimuon data

Non-resonant DY 7-TeV ATLAS data

ATLAS (7 TeV, 4.6 fb⁻¹) 1612.03016



- Complementary constraint on PDFs → improved quark disentangling

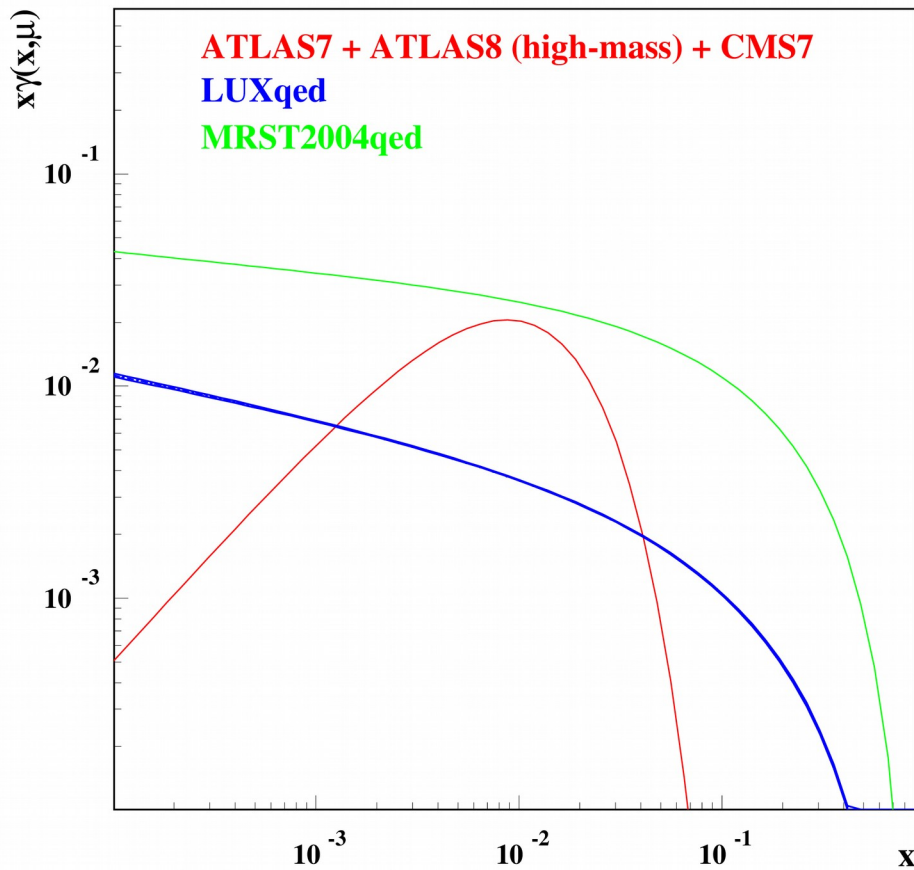
$$\sigma_{\text{DY}} \sim q_u^2 u(x_2) \bar{u}(x_1) + q_d^2 d(x_2) \bar{d}(x_1)$$

$$\sigma_{\text{DIS}} \sim q_u^2 u(x_2) + q_d^2 d(x_2)$$

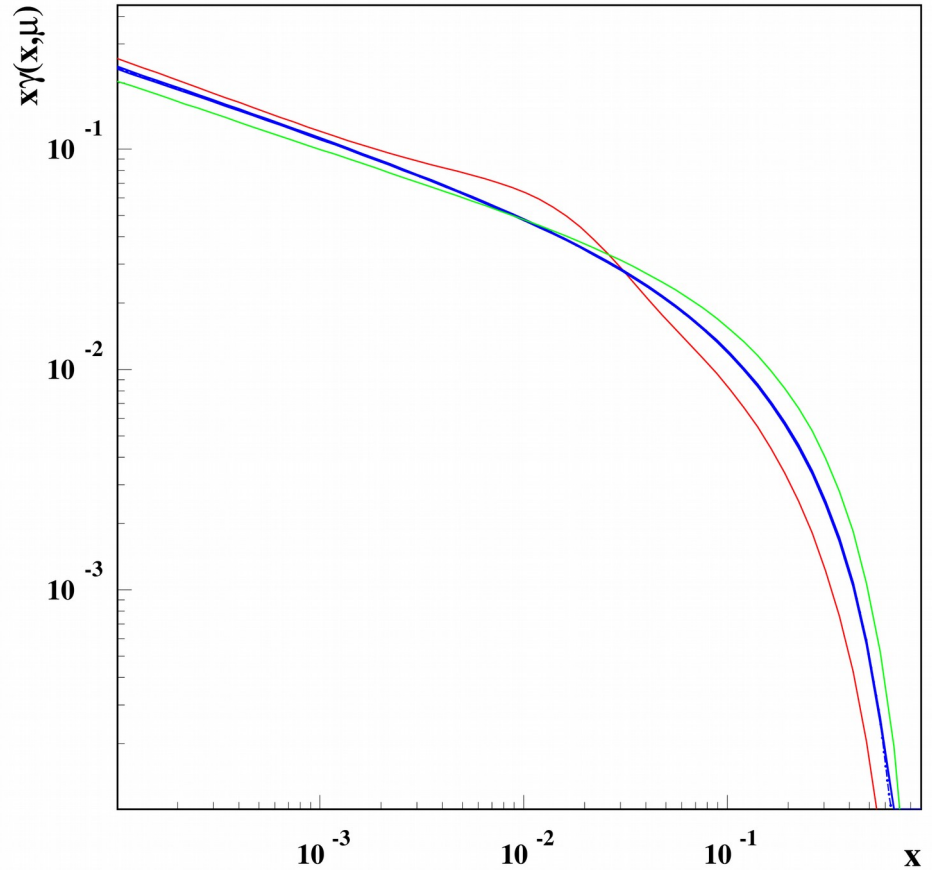
- Additional photon-photon contribution (in LO) improves agreement → photon distribution can be extracted from the data

Photon PDF fitted to the DY data

$\mu=3$ GeV



$\mu=100$ GeV



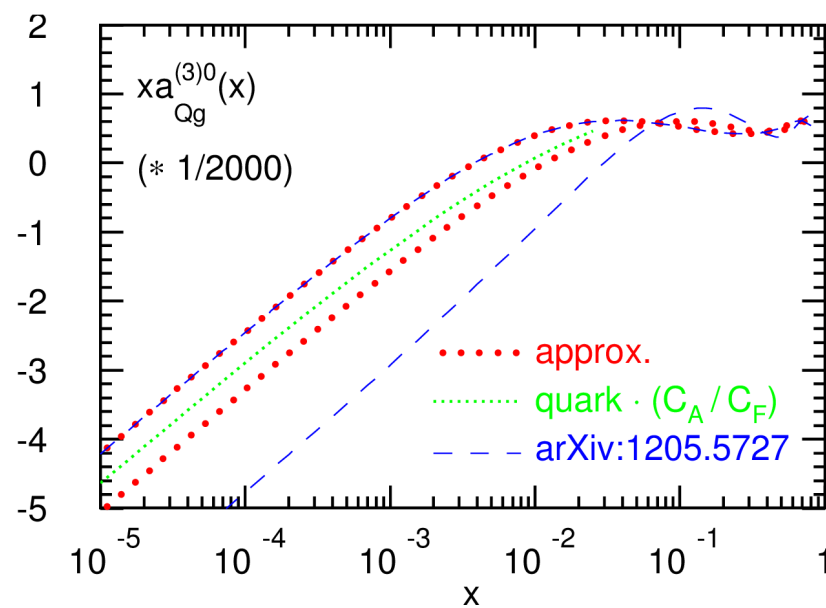
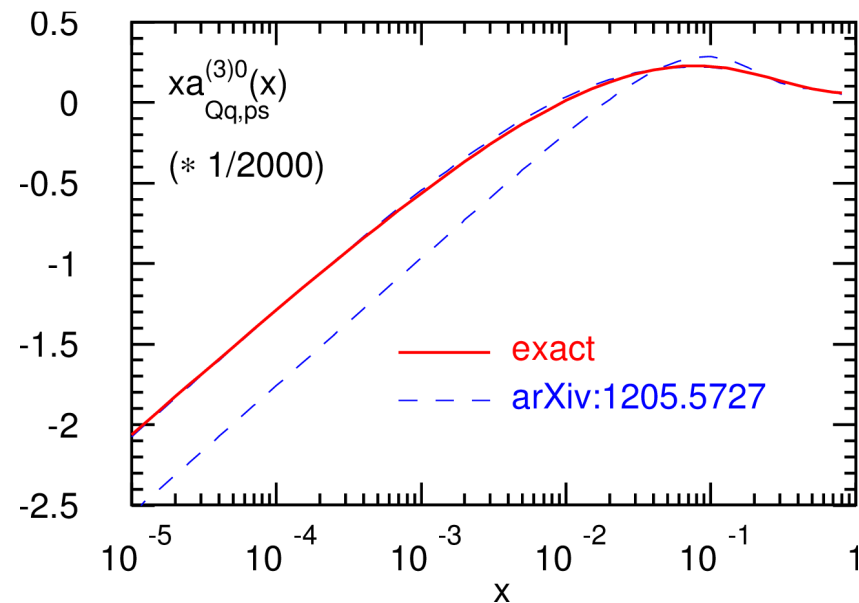
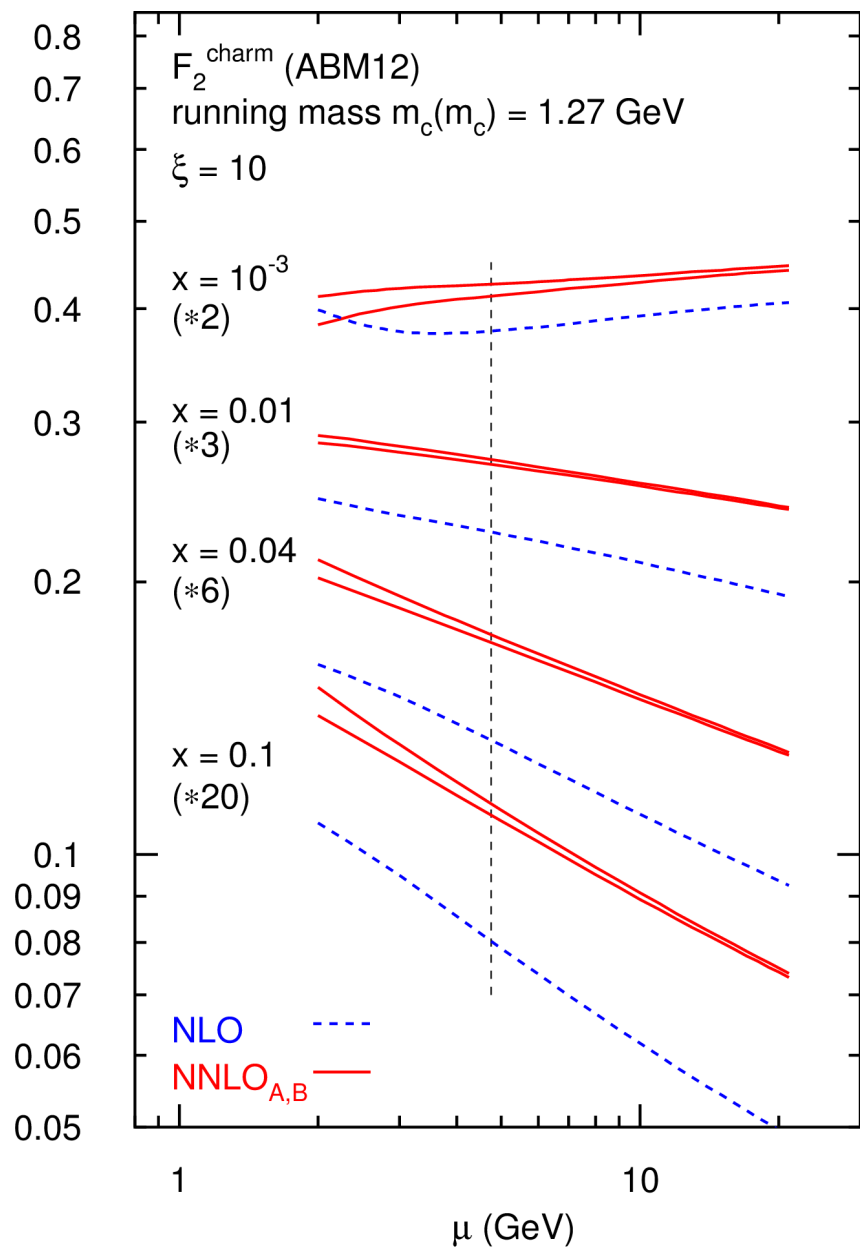
Data set	χ^2/NDP
ATLAS7 - 1612.03016	68/61
ATLAS8 (high-mass) - 1606.01736	58/48
CMS7 - 1310.7291	192/32

Quite different evolution input for the available photon distributions. Reduces at large scales, however still sensitive to the quark distributions (cf. PDF4LHC issue in LUXqed)

Manohar, Nason, Salam, Zanderighi hep-ph/1708.01256

The (quasi)-elastic contribution is not considered – conceptual difference with LUXqed

Recent progress in FFN scheme Wilson coefficients

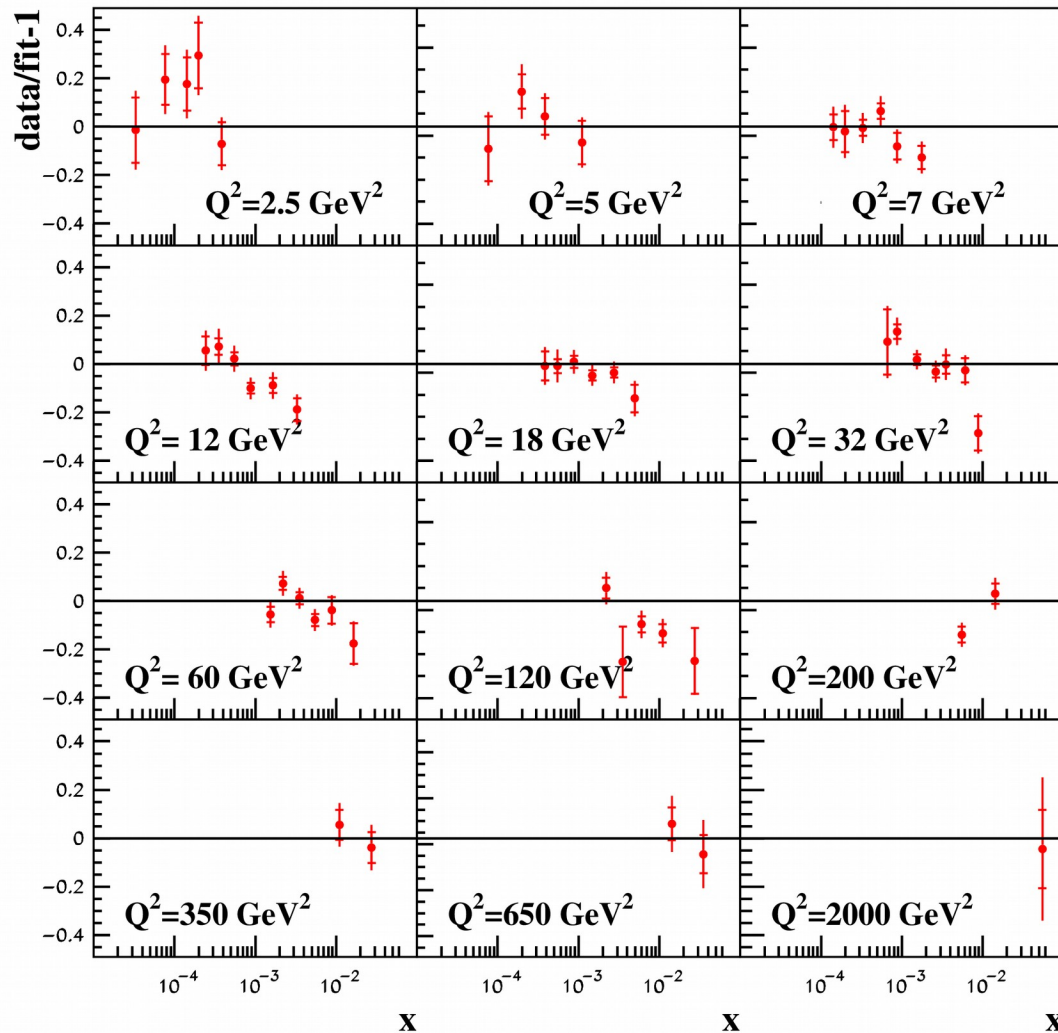


Update with the pure singlet massive OMEs \rightarrow improved theoretical uncertainties

HERA charm data and m_c

H1, ZEUS EPJC 78, 473 (2018)

HERA I+II (ep --> e charm X)



Theory: FFN scheme, running mass definition

$$m_c(m_c) = 1.250 \pm 0.019 (\text{exp.}) \text{ GeV}$$

ABMP16upd

$$m_c(m_c) = 1.252 \pm 0.018 (\text{exp.}) \text{ GeV}$$

ABMP16

$$m_c(\text{pole}) \sim 1.9 \text{ GeV (NNLO)}$$

Marquard et al. PRL 114, 142002 (2015)

$$m_c(m_c) = 1.246 \pm 0.023 (\text{h.o.}) \text{ GeV NNLO}$$

Kiyo, Mishima, Sumino PLB 752, 122 (2016)

$$m_c(m_c) = 1.279 \pm 0.008 \text{ GeV}$$

Kühn, LoopsLegs2018

Good consistency with the earlier results and other determinations → further confirmation of the FFN scheme relevance for the HERA kinematics

Higher twists in DIS: generalities

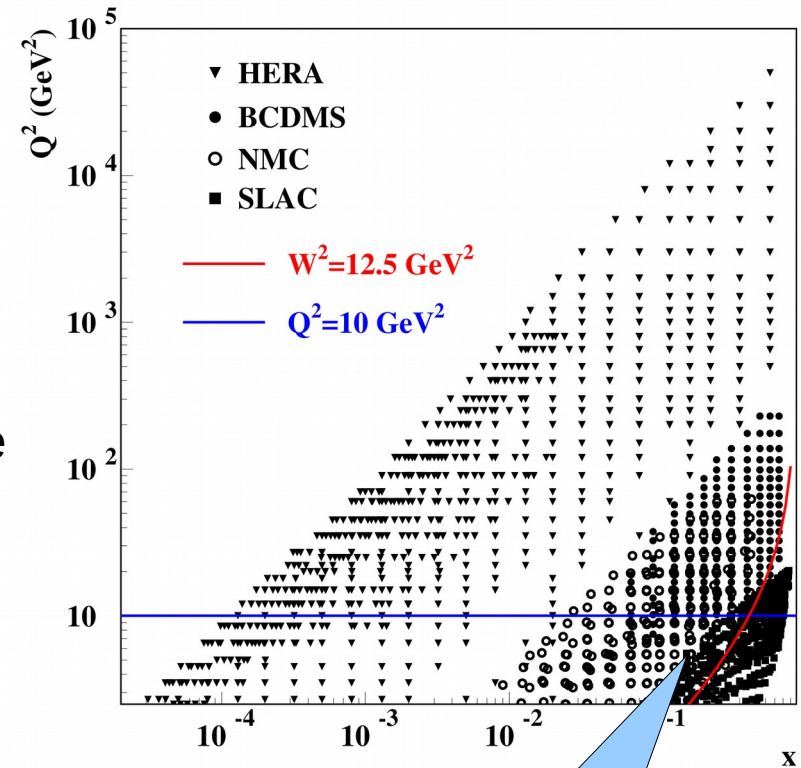
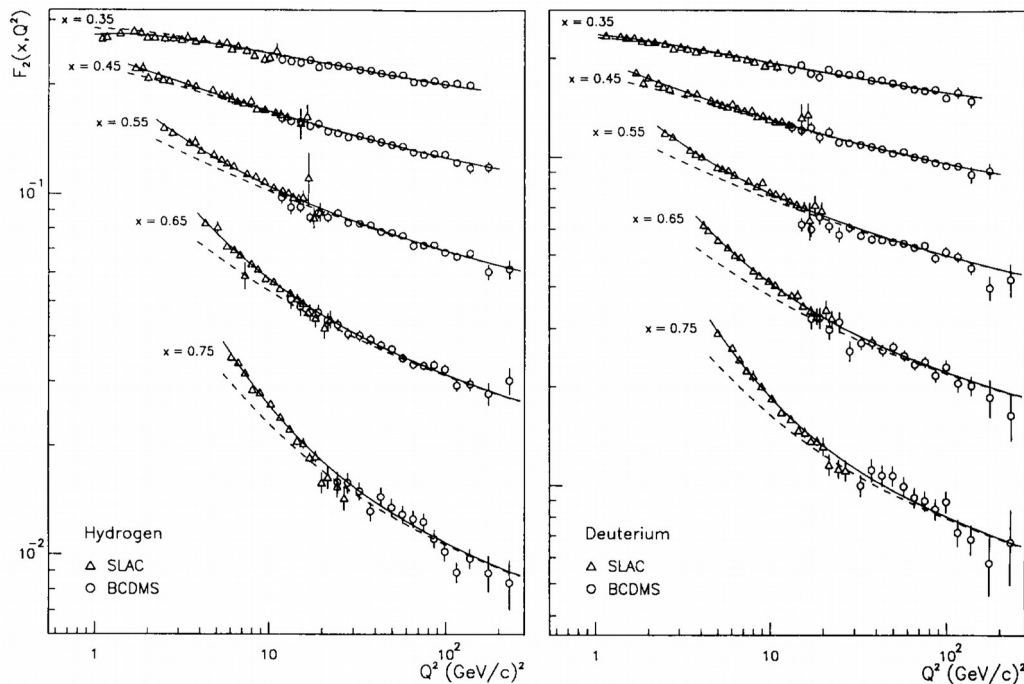
Operator product expansion:

$$F_{2,T} = F_{2,T}(\text{leading twist}) + H_{2,T}(x)/Q^2 + \dots - \text{additive}$$

- The only one in accordance with QCD

$$F_{2,T} = F_{2,T}(\text{leading twist}) (1 + h_{2,T}(x)/Q^2 + \dots) - \text{multiplicative}$$

- For multiplicative form the LT anomalous dimensions strongly affect the HT terms at small x

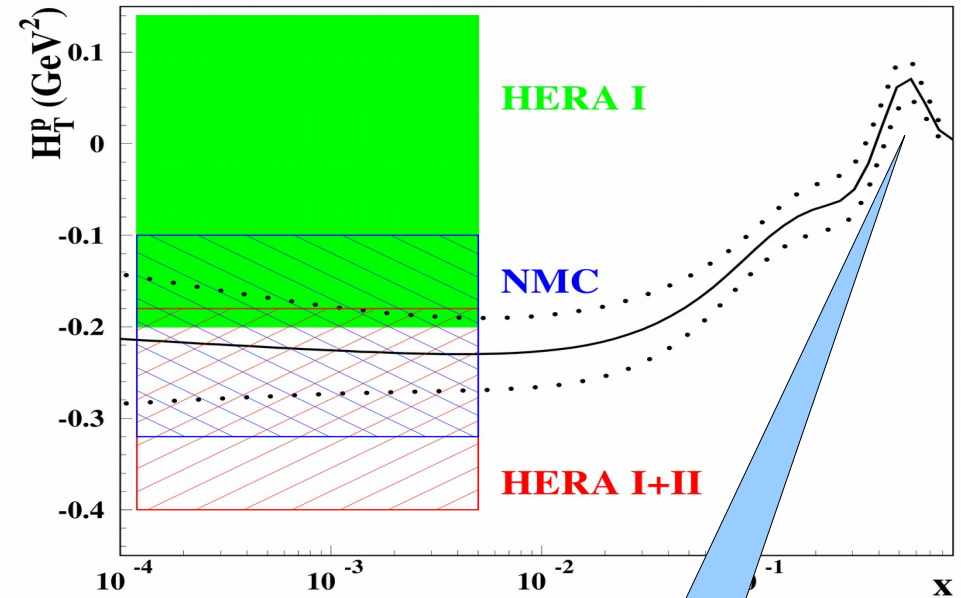
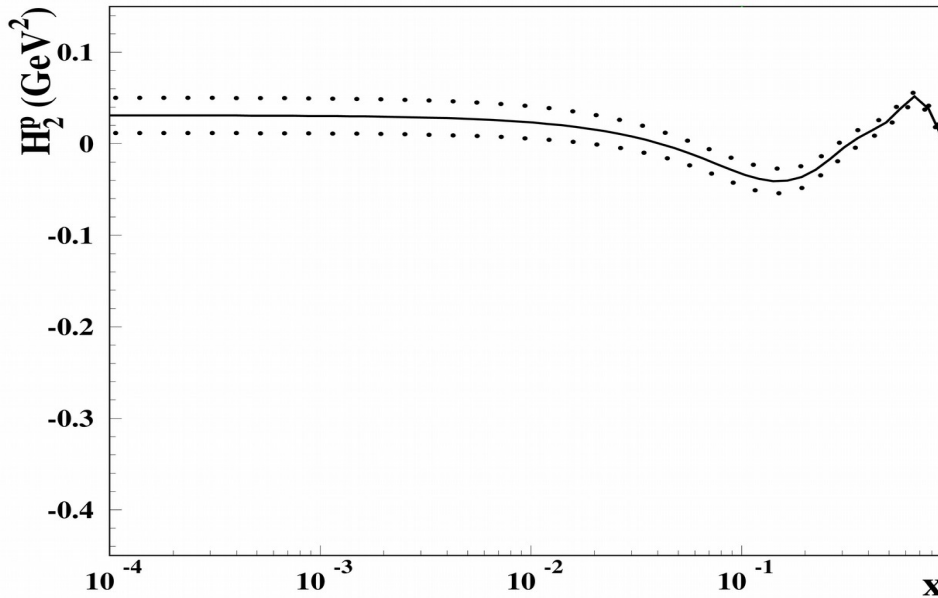


High twists appear in the DIS data at large x (equiv. W) and/or small Q²

High twists at small x

$$F_{2,T} = F_{2,T}(\text{leading twist}) + H_{2,T}(x)/Q^2$$

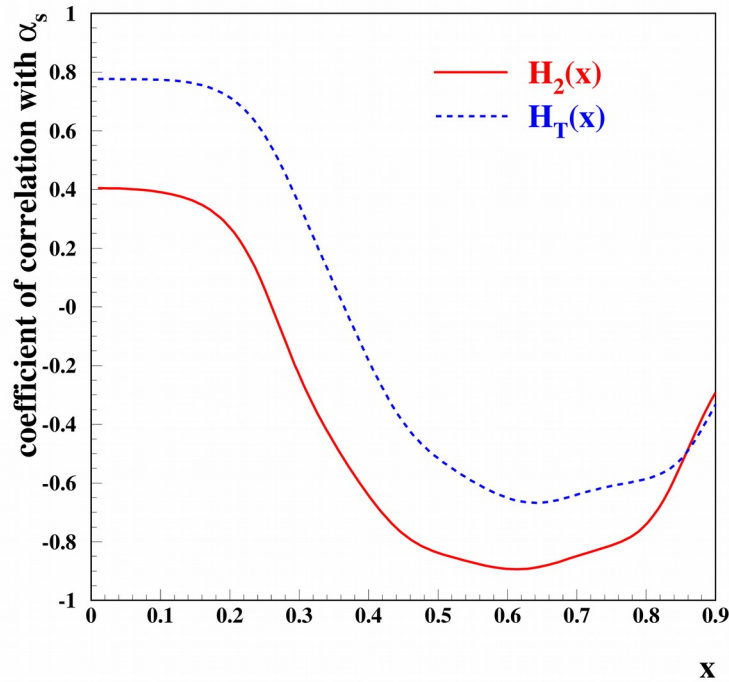
$$H(x) = x^h P(x)$$



Controlled by
SLAC data

- $H_T(x)$ continues a trend observed at larger x
- $H_2(x)$ is comparable to 0 at small x
- $h_T = 0.05 \pm 0.07 \rightarrow$ slow vanishing at $x \rightarrow 0$
- Alternative explanations are considered: resummation, saturation, data defects, etc.

Correlation of α_s with twist-4 terms



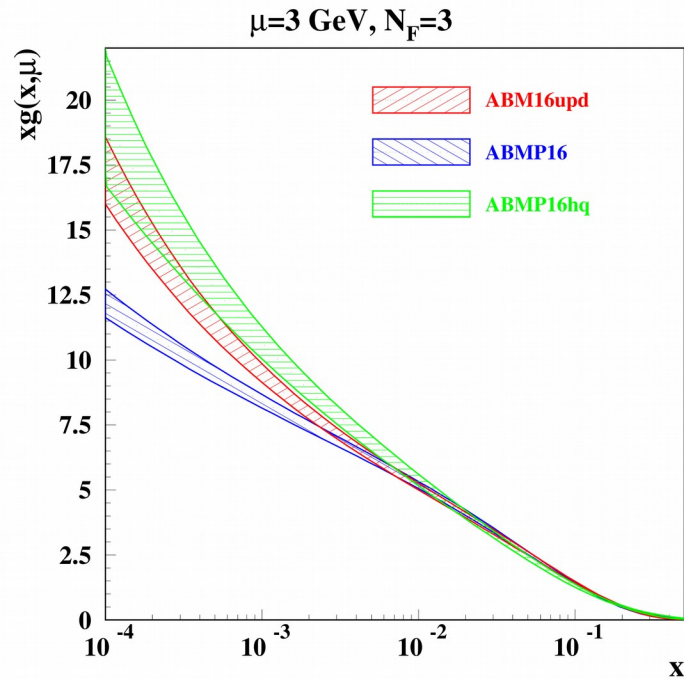
- The value of α_s and twist-4 terms are strongly Correlated both at large and at small x
- With HT=0 the errors are reduced \rightarrow no uncertainty due to HTs
- With account of the HT terms the value of α_s is stable with respect to the cuts

MRST: $\alpha_s(M_Z)=0.1153(20)$ (NNLO)
 $(W^2 > 15 \text{ GeV}^2, Q^2 > 10 \text{ GeV}^2)$

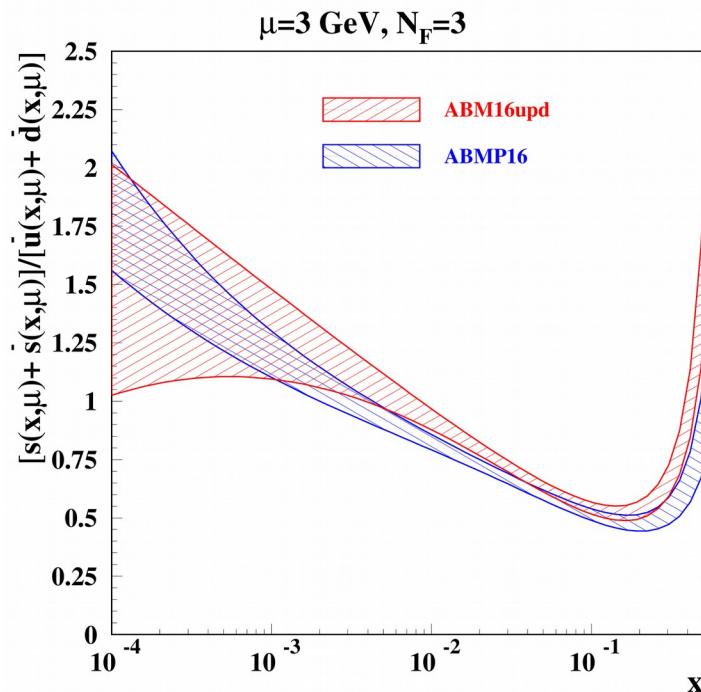
fit ansatz		$\alpha_s(M_Z)$	
higher twist modeling	cuts on DIS data	NLO	NNLO
higher twist fitted	$Q^2 > 2.5 \text{ GeV}^2, W > 1.8 \text{ GeV}$	0.1191(11)	0.1147(8)
higher twist fixed at 0	$Q^2 > 10 \text{ GeV}^2, W^2 > 12.5 \text{ GeV}^2$	0.1212(9)	0.1153(8)
	$Q^2 > 15 \text{ GeV}^2, W^2 > 12.5 \text{ GeV}^2$	0.1201(11)	0.1141(10)
	$Q^2 > 25 \text{ GeV}^2, W^2 > 12.5 \text{ GeV}^2$	0.1208(13)	0.1138(11)

A stringent cut on Q is necessary for the fit with HT=0

Small-x PDF with stringent cut on Q,W



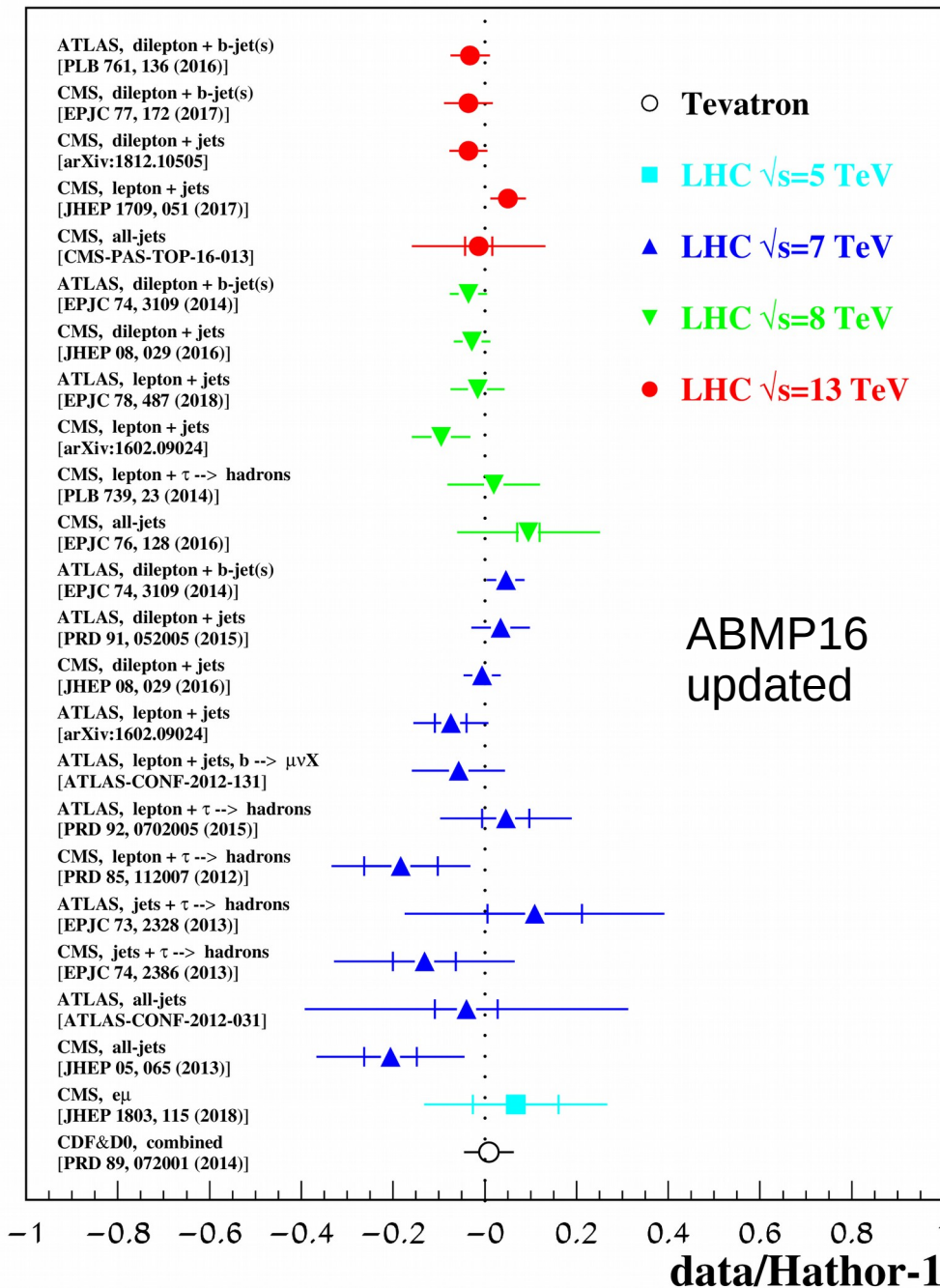
- Gluon goes higher due to more stringent cut on Q^2 (impact of the power corrections, resummations, etc. is reduced)
- Updated charm/beauty data are consistent with such an enhancement



- Strange sea suppression factor goes lower at small x , consistent with 1 within errors
- At moderate x the strange sea is still suppressed, although integral suppression factor $\kappa_s(20 \text{ GeV}^2)=0.71(3)$, a little larger than $0.66(3)$ for ABMP16 fit due to recent ATLAS data included

Impact of t-quark data

$\sigma(\bar{t}tX)$



- Running t-quark mass is determined simultaneously with PDFs

$$m_t(m_t) = 160.9 \pm 1.1 \text{ GeV}$$

$$m_t(\text{pole}) = 170.4 \pm 1.2 \text{ GeV}$$

$$m_t(\text{MC}) \sim 172.5 \text{ GeV from LHC}$$

$$m_t(\text{pole}) = 170.5 \pm 0.8 \text{ GeV}$$

CMS hep-ex/1904.05237

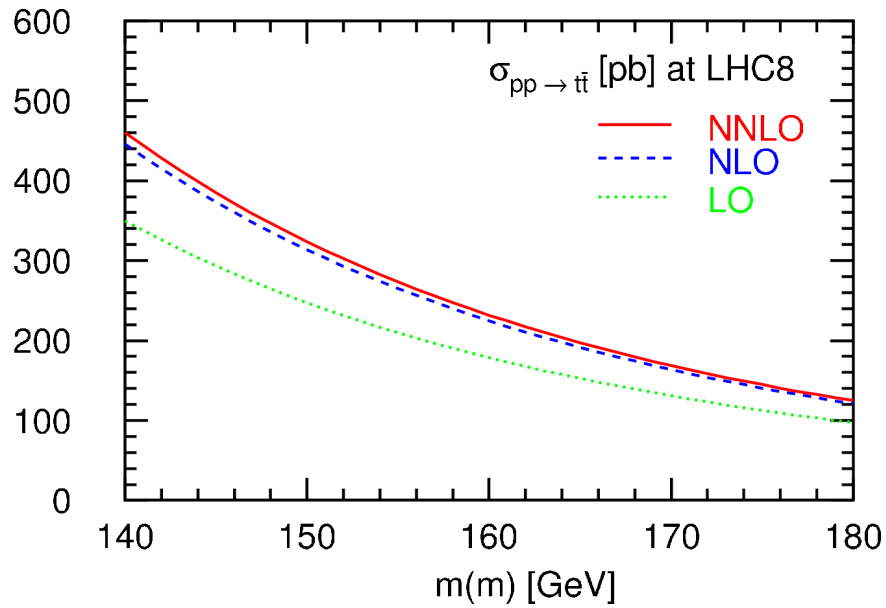
$$m_t(\text{pole}) = 171.1 \pm 1.1 \text{ GeV}$$

ATLAS hep-ex/1905.02302

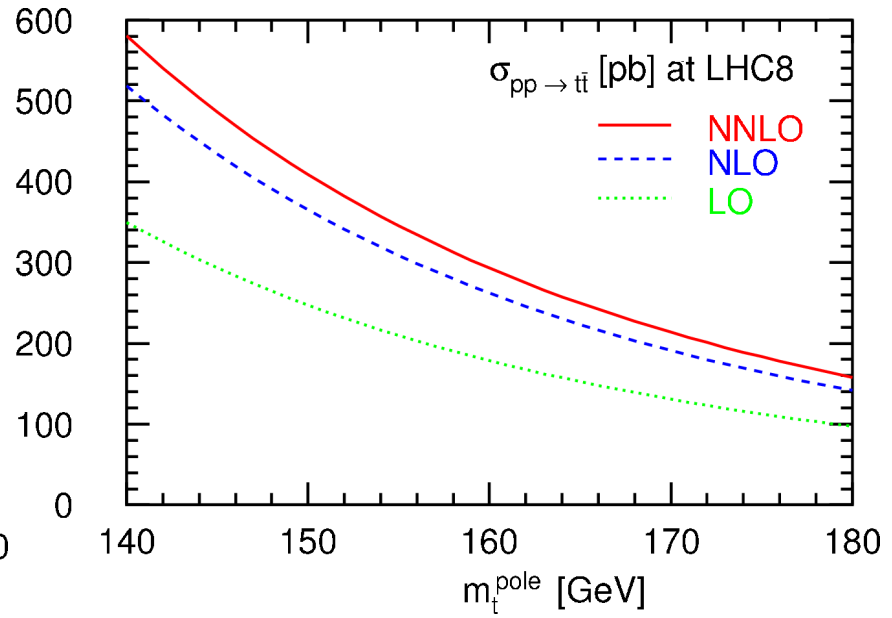
(Hoang et al. try to quantify the Difference between $m_t(\text{MC})$ and other determinations)

Impact of the t-quark data on the ABMP16 fit

MSbar



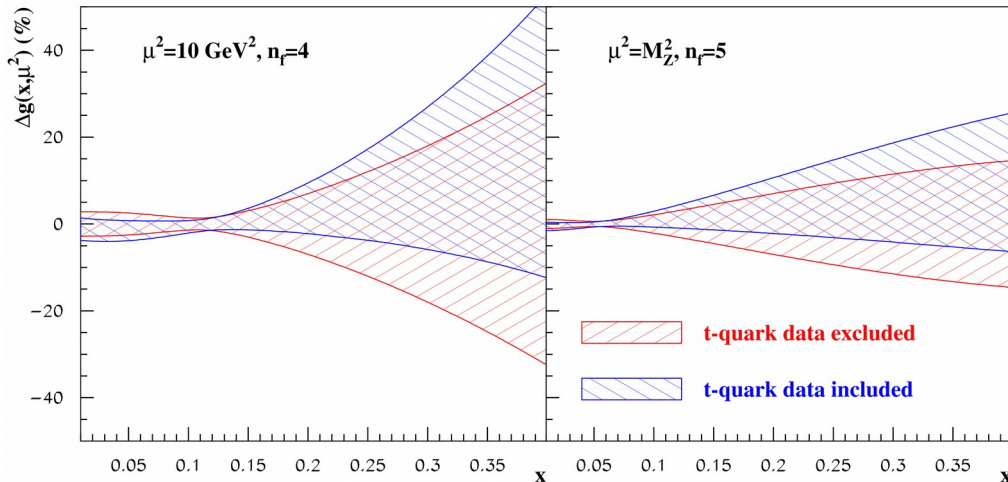
Pole



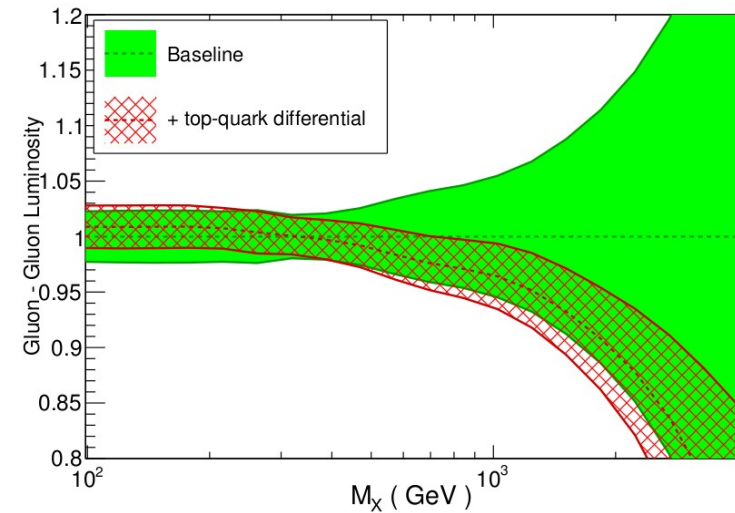
HATHOR (NNLO terms are checked with TOP++)

Langenfeld, Moch, Uwer PRD 80, 054009 (2009)

Running mass definition provides nice perturbative stak



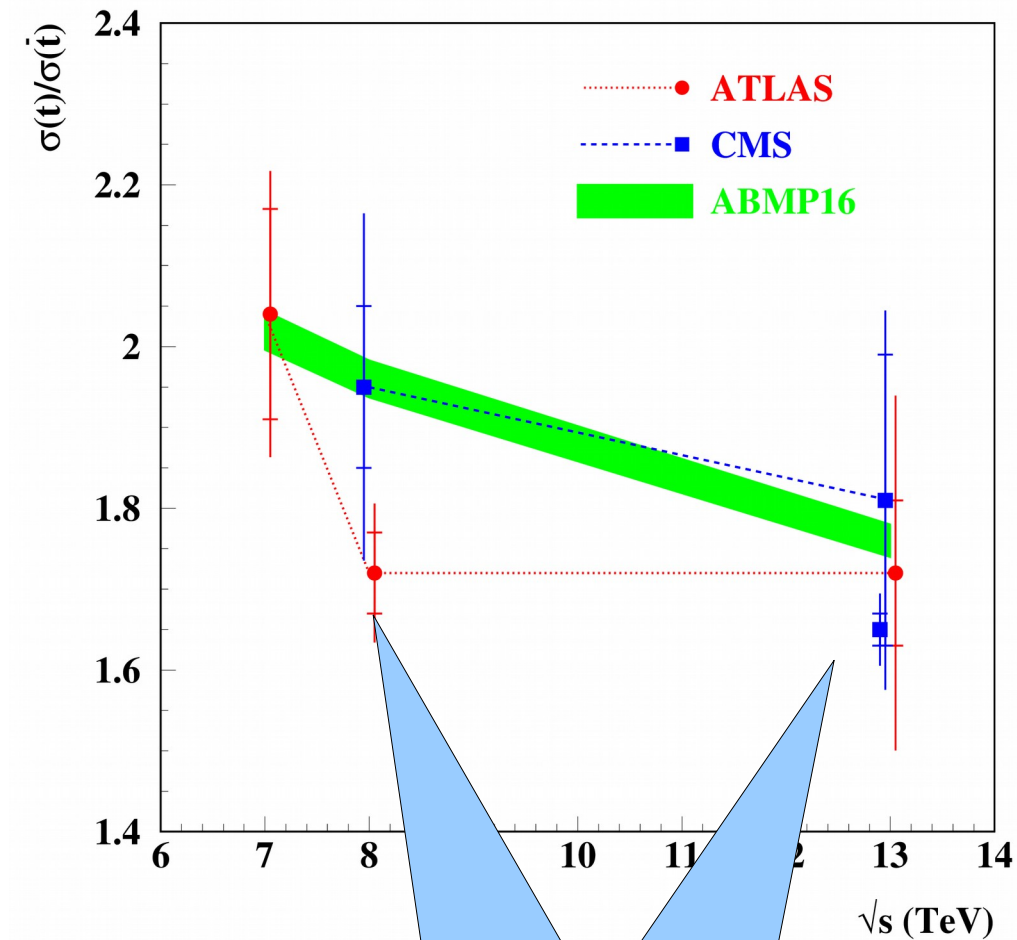
NNLO, global fits, LHC 13 TeV



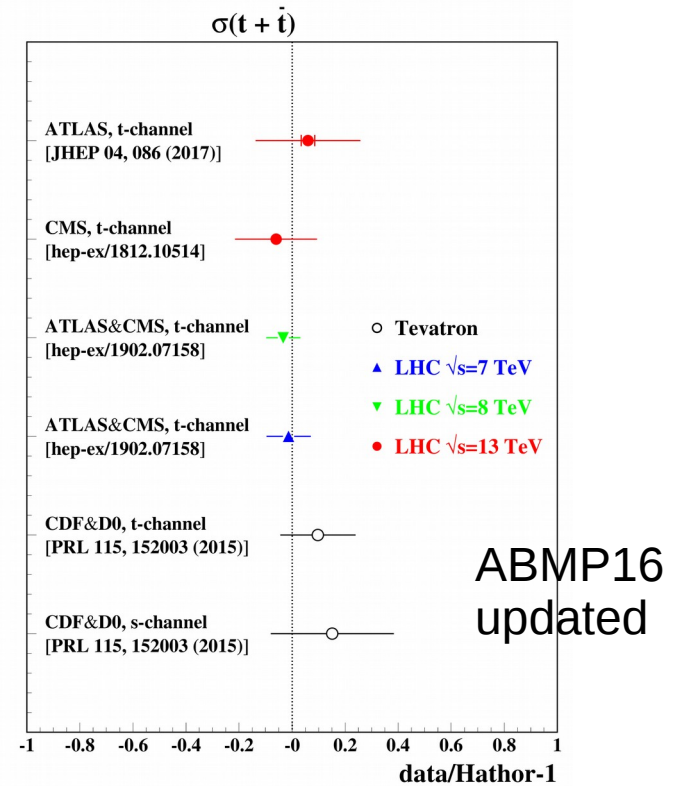
Czakon et al., JHEP 1704, 044 (2017)

fastNLO

t-quark: single production



Small errors due to cancellation of theor. unc. in case the MC version is fixed; they are much larger if different MCs are considered



- The single-top data are sensitive to the u/d ratio, however in general they are not competitive with the DY constraints
- The only window opens when the hadronization MC is fixed and the modeling errors cancel in the ratio → model dependent result
- The comparison can be also inverted in order to discriminate hadronization models

Summary and outlook

- Steady improvement in the quark PDFs' determination due to DY LHC data
 - disentangling d- and u-quark distributions at small x
 - improvement in the large-x d- and u-quark distributions: impact of the forward LHC and Tevatron data; no enhancement in d/u at large x is observed
 - somewhat enhanced strange distribution at small x, however, the large-x enhancement reported by ATLAS seems to be an artifact of the PDF shape used
- The HERA inclusive and semi-inclusive data allow to distinguish between the FFN and VFN factorization schemes in DIS. The FFN scheme provides nice agreement with existing data and

$$m_c(m_c)=1.250\pm 0.019(\text{exp.})-0.01(\text{th.}) \text{ GeV},$$

in a good agreement with other determinations.

- t-quark data are emerging at NNLO fits with a progress of the computational tools

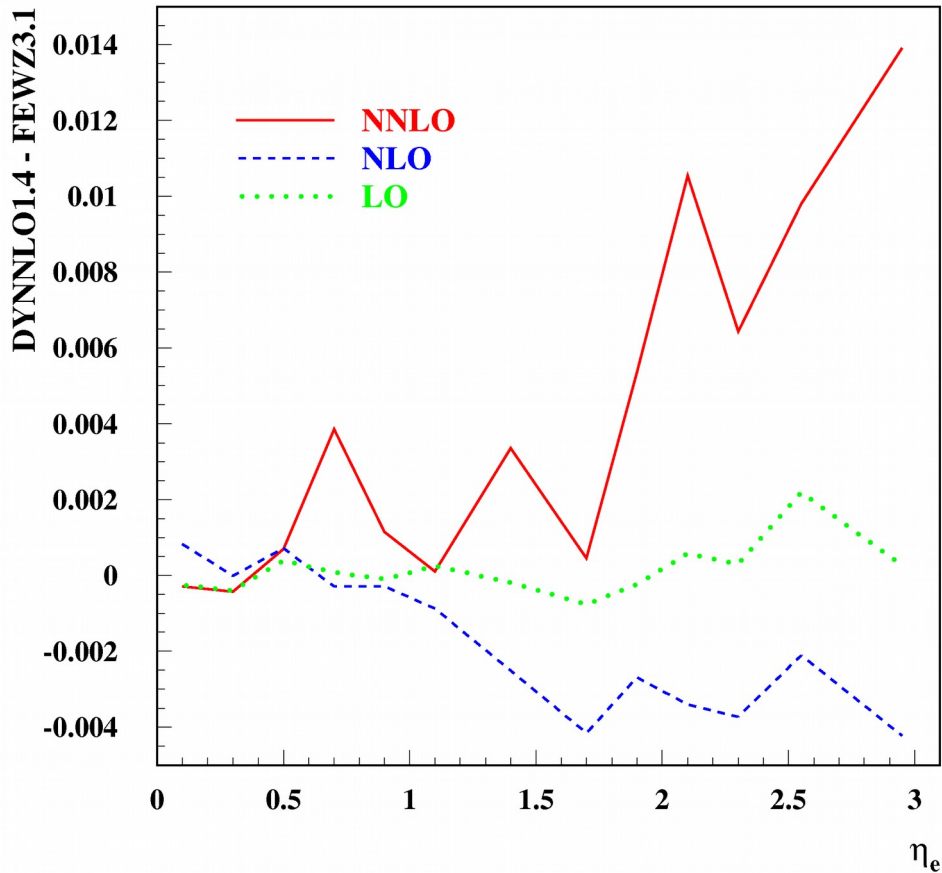
$$m_t(m_t)= 160.9\pm 1.1 \text{ GeV}$$

$$m_t(\text{pole})=170.4\pm 1.2 \text{ GeV}$$

EXTRAS

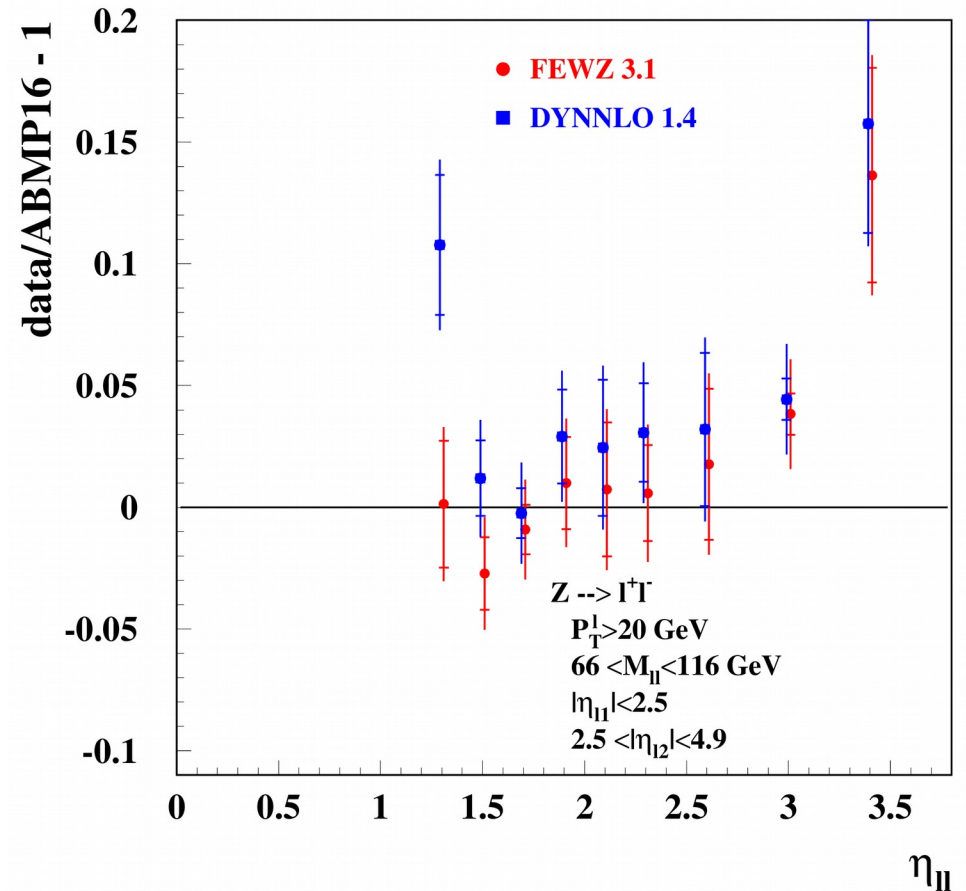
NNLO tools benchmarking

$A_e^W, D0$ (1.96 TeV, 9.7 fb⁻¹) 1412.2862



Yannick Ulrich, Bachelor thesis, Univ. of Hamburg 2015

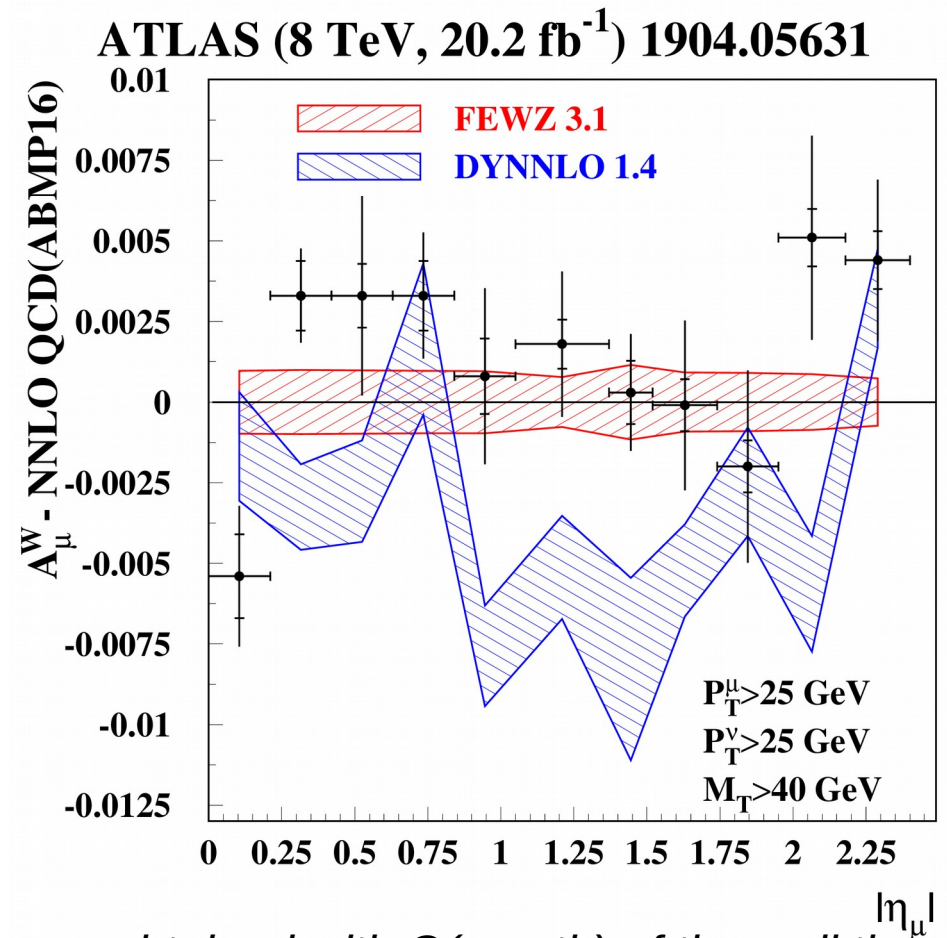
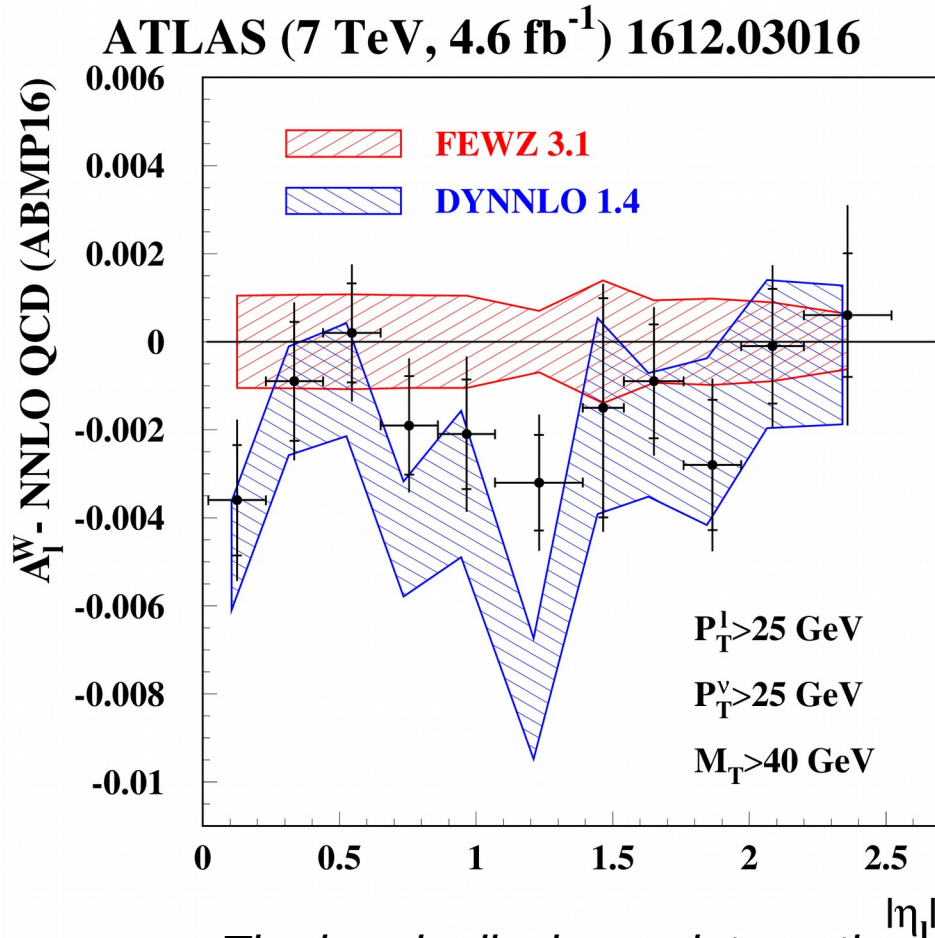
ATLAS (7 TeV, 4.6 fb⁻¹) 1612.03016



DYNNLO-FEWZ difference not fully understood; further benchmarking is needed

Walker, this conference

NNLO tools' benchmarking



The bands display an integration accuracy obtained with $O(\text{month})$ of the wall time

- The FEWZ predictions somewhat overshoot the data at 7 TeV, while the DYNNLO ones go lower and are in better agreement with the measurements
- At 8 TeV the tendency is different: The FEWZ predictions somewhat undershoot the data and the DYNNLO ones go essentially lower
- FEWZ predictions demonstrate better overall agreement with the data – routinely used in the fit

TABLE II. The list of DIS and DY data used in the current analysis with the collider data listed first. The top-quark production data are detailed in Tables III and IV.

Experiment	Beam (E_b) or center-of-mass energy (\sqrt{s})	\mathcal{L} (1/fb)	Process	Kinematic cuts used in the present analysis (cf. original references for notations)	Ref.
<i>DIS</i>					
HERA I + II	$\sqrt{s} = 0.225 \div 0.32$ TeV	0.5	$e^\pm p \rightarrow e^\pm X$	$2.5 \leq Q^2 \leq 50000 \text{ GeV}^2$, $2.5 \times 10^{-5} \leq x \leq 0.65$	[4]
BCDMS	$E_b = 100 \div 280 \text{ GeV}$		$e^\pm p \rightarrow \nu^- X$	$200 \leq Q^2 \leq 50000 \text{ GeV}^2$, $1.3 \times 10^{-2} \leq x \leq 0.40$	[61]
NMC	$E_b = 90 \div 280 \text{ GeV}$		$\mu^\pm p \rightarrow \mu^\pm X$	$7 < Q^2 < 230 \text{ GeV}^2$, $0.07 \leq x \leq 0.75$	[60]
SLAC-49a	$E_b = 7 \div 20 \text{ GeV}$		$e^- p \rightarrow e^- X$	$2.5 \leq Q^2 < 8 \text{ GeV}^2$, $0.1 < x < 0.8$, $W \geq 1.8 \text{ GeV}$	[54]
SLAC-49b	$E_b = 4.5 \div 18 \text{ GeV}$		$e^- p \rightarrow e^- X$	$2.5 \leq Q^2 < 20 \text{ GeV}^2$, $0.1 < x < 0.9$, $W \geq 1.8 \text{ GeV}$	[62]
SLAC-87	$E_b = 8.7 \div 20 \text{ GeV}$		$e^- p \rightarrow e^- X$	$2.5 \leq Q^2 < 20 \text{ GeV}^2$, $0.3 < x < 0.9$, $W \geq 1.8 \text{ GeV}$	[54]
SLAC-89b	$E_b = 6.5 \div 19.5 \text{ GeV}$		$e^- p \rightarrow e^- X$	$2.5 \leq Q^2 \leq 19 \text{ GeV}^2$, $0.17 < x < 0.9$, $W \geq 1.8 \text{ GeV}$	[56]
<i>DIS heavy-quark production</i>					
HERA I + II	$\sqrt{s} = 0.32 \text{ TeV}$		$e^\pm p \rightarrow e^\pm cX$	$2.5 \leq Q^2 \leq 2000 \text{ GeV}^2$, $2.5 \times 10^{-5} \leq x \leq 0.05$	[63]
H1	$\sqrt{s} = 0.32 \text{ TeV}$	0.189	$e^\pm p \rightarrow e^\pm bX$	$5 \leq Q^2 \leq 2000 \text{ GeV}^2$, $2 \times 10^{-4} \leq x \leq 0.05$	[15]
ZEUS	$\sqrt{s} = 0.32 \text{ TeV}$	0.354	$e^\pm p \rightarrow e^\pm bX$	$6.5 \leq Q^2 \leq 600 \text{ GeV}^2$, $1.5 \times 10^{-4} \leq x \leq 0.035$	[16]
CCFR	$87 \lesssim E_b \lesssim 333 \text{ GeV}$		$\nu^- N \rightarrow \mu^\pm cX$	$1 \leq Q^2 < 170 \text{ GeV}^2$, $0.015 \leq x \leq 0.33$	[64]
CHORUS	$\langle E_b \rangle \approx 27 \text{ GeV}$		$\nu N \rightarrow \mu^\pm cX$		[18]
NOMAD	$6 \leq E_b \leq 300 \text{ GeV}$		$\nu N \rightarrow \mu^\pm cX$	$1 \leq Q^2 < 20 \text{ GeV}^2$, $0.02 \lesssim x \leq 0.75$	[17]
NuTeV	$79 \lesssim E_b \lesssim 245 \text{ GeV}$		$\nu^- N \rightarrow \mu^\pm cX$	$1 \leq Q^2 < 120 \text{ GeV}^2$, $0.015 \leq x \leq 0.33$	[64]
<i>DY</i>					
ATLAS	$\sqrt{s} = 7 \text{ TeV}$	0.035	$pp \rightarrow W^\pm X \rightarrow l^\pm \nu X$	$p_T^l > 20 \text{ GeV}$, $p_T^\nu > 25 \text{ GeV}$, $m_T > 40 \text{ GeV}$	[67]
	$\sqrt{s} = 13 \text{ TeV}$	0.081	$pp \rightarrow ZX \rightarrow l^+ l^- X$ $pp \rightarrow W^\pm X \rightarrow l^\pm \nu X$ $pp \rightarrow ZX \rightarrow l^+ l^- X$	$p_T^l > 20 \text{ GeV}$, $66 < m_{ll} < 116 \text{ GeV}$ $p_T^\nu > 25 \text{ GeV}$, $m_T > 50 \text{ GeV}$ $p_T^l > 25 \text{ GeV}$, $66 < m_{ll} < 116 \text{ GeV}$	[26]
CMS	$\sqrt{s} = 7 \text{ TeV}$	4.7	$pp \rightarrow W^\pm X \rightarrow \mu^\pm \nu X$	$p_T^\mu > 25 \text{ GeV}$	[24]
	$\sqrt{s} = 8 \text{ TeV}$	18.8	$pp \rightarrow W^\pm X \rightarrow \mu^\pm \nu X$	$p_T^\mu > 25 \text{ GeV}$	[25]
DØ	$\sqrt{s} = 1.96 \text{ TeV}$	7.3	$\bar{p}p \rightarrow W^\pm X \rightarrow \mu^\pm \nu X$	$p_T^\mu > 25 \text{ GeV}$, $E_T > 25 \text{ GeV}$	[23]
		9.7	$\bar{p}p \rightarrow W^\pm X \rightarrow e^\pm \nu X$	$p_T^\mu > 25 \text{ GeV}$, $E_T > 25 \text{ GeV}$	[22]
LHCb	$\sqrt{s} = 7 \text{ TeV}$	1	$pp \rightarrow W^\pm X \rightarrow \mu^\pm \nu X$	$p_T^\mu > 20 \text{ GeV}$	[19]
	$\sqrt{s} = 8 \text{ TeV}$	2	$pp \rightarrow ZX \rightarrow \mu^+ \mu^- X$	$p_T^\mu > 20 \text{ GeV}$, $60 < m_{\mu\mu} < 120 \text{ GeV}$	[21]
		2.9	$pp \rightarrow W^\pm X \rightarrow \mu^\pm \nu X$ $pp \rightarrow ZX \rightarrow \mu^+ \mu^- X$	$p_T^\mu > 20 \text{ GeV}$ $p_T^\mu > 20 \text{ GeV}$, $60 < m_{\mu\mu} < 120 \text{ GeV}$	[20]
FNAL-605	$E_b = 800 \text{ GeV}$		$pCu \rightarrow \mu^+ \mu^- X$	$7 \leq M_{\mu\mu} \leq 18 \text{ GeV}$	[68]
FNAL-866	$E_b = 800 \text{ GeV}$		$pp \rightarrow \mu^+ \mu^- X$ $pD \rightarrow \mu^+ \mu^- X$	$4.6 \leq M_{\mu\mu} \leq 12.9 \text{ GeV}$	[69]

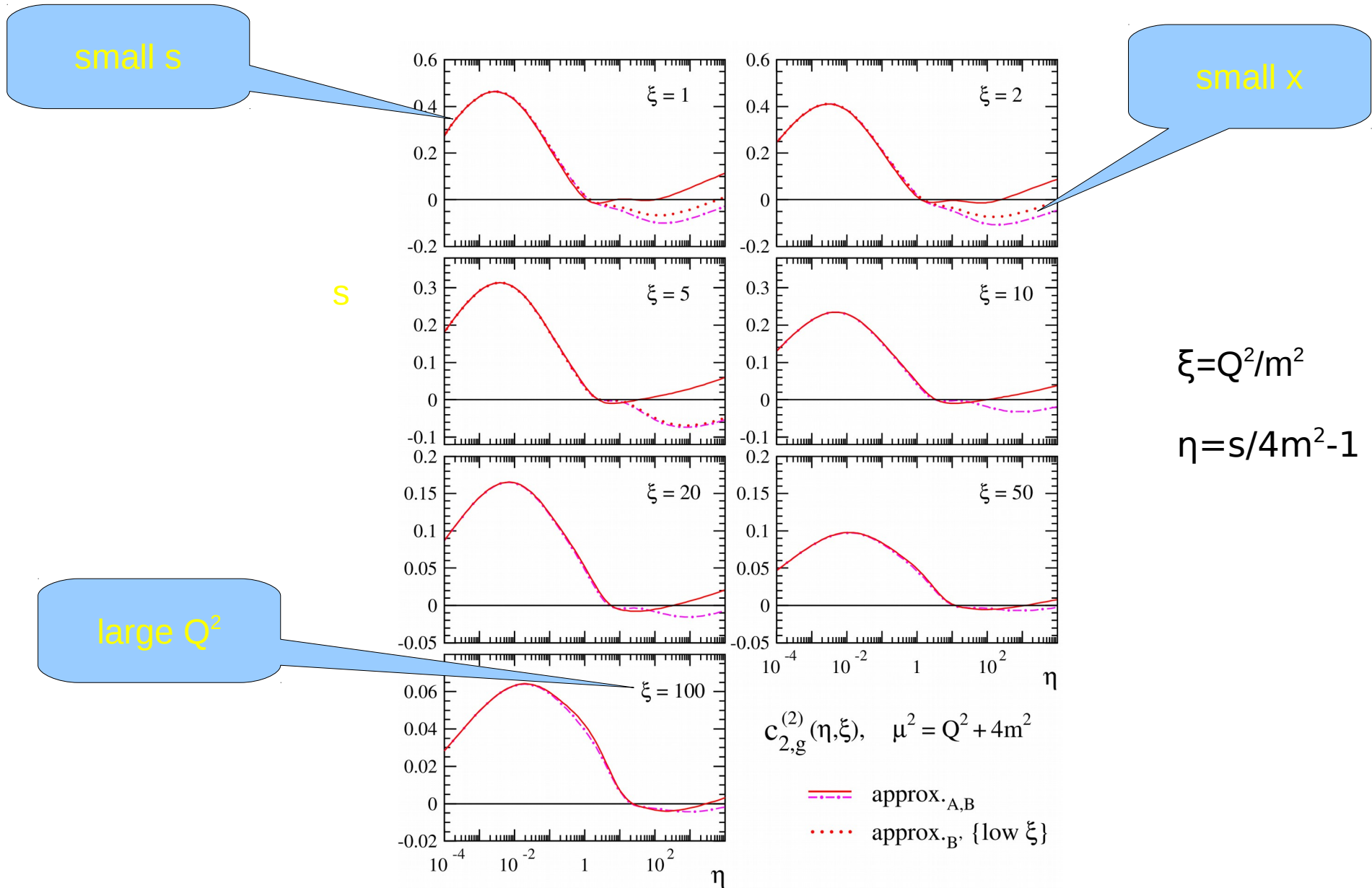
TABLE III. The data on the $t\bar{t}$ -production cross section from the LHC used in the present analysis. The errors given are combinations of the statistical and systematic ones. An additional error of 1.4, 3.3, 4.2 and 12 pb due to the beam energy uncertainty applies to all entries for the collision energy of $\sqrt{s} = 5, 7, 8$ and 13 TeV, respectively. The quoted values are rounded for the purpose of a compact presentation.

\sqrt{s} (TeV)	Experiment	Cross section (pb)						
		5		7		8		13
		CMS	ATLAS	CMS	ATLAS	CMS	ATLAS	CMS
Decay mode	dilepton + b -jet(s)		183 ± 6 [36]		243 ± 8 [36]		818 ± 36 [37]	792 ± 43 [38]
	dilepton + jets		181 ± 11 [33]	174 ± 6 [34]		245 ± 9 [34]		746 ± 86 [35]
	lepton + jets			162 ± 14 [39]	260 ± 24 [40]	229 ± 15 [39]		836 ± 133 [41]
	lepton + jets, $b \rightarrow \mu\nu X$		165 ± 38 [42]					
	lepton + $\tau \rightarrow$ hadrons		183 ± 25 [43]	143 ± 26 [44]		257 ± 25 [51]		
	jets + $\tau \rightarrow$ hadrons		194 ± 49 [46]	152 ± 34 [47]				
	all-jets		168 ± 60 [48]	139 ± 28 [49]		276 ± 39 [45]		834^{+123}_{-109} [50]
	$e\mu$		82 ± 23 [52]					

TABLE IV. The data on single-top production in association with a light quark q or \bar{b} -quark from the LHC and Tevatron used in the present analysis. The errors given are combinations of the statistical, systematic, and luminosity ones.

Experiment	ATLAS			CMS			CDF&DØ
	7	8	13	7	8	13	
\sqrt{s} (TeV)	7	8	13	7	8	13	1.96
Final states	tq	tq	tq	tq	tq	tq	$tq, t\bar{b}$
Reference	[27]	[28]	[29]	[30]	[31]	[32]	[53]
Luminosity (1/fb)	4.59	20.3	3.2	2.73	19.7	2.3	9.7×2
Cross section (pb)	68 ± 8	82.6 ± 12.1	247 ± 46	67.2 ± 6.1	83.6 ± 7.7	232 ± 30.9	$3.30^{+0.52}_{-0.40}$ (sum)

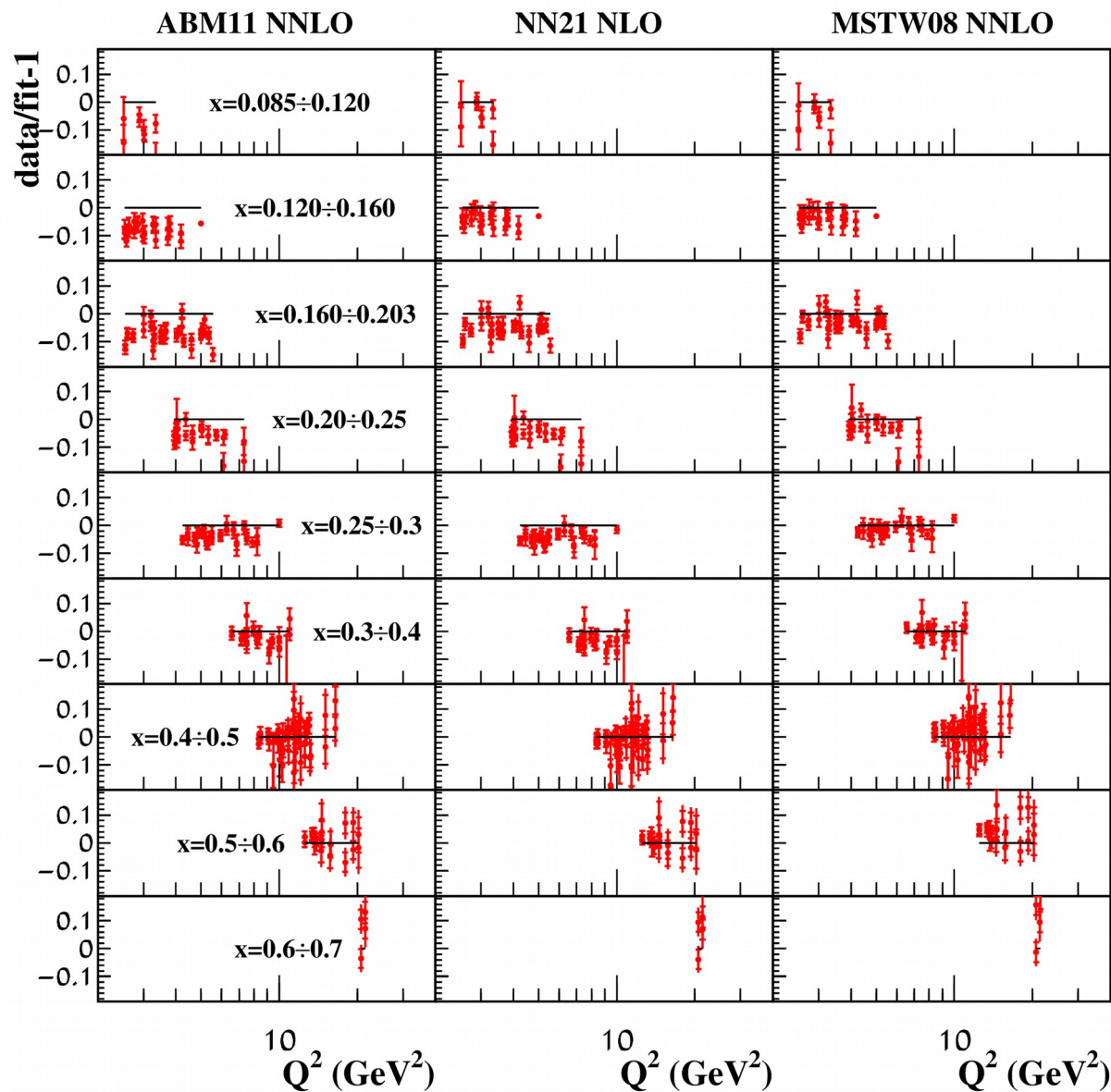
Modeling NNLO massive coefficients



Combination of the threshold corrections (small s), high-energy limit (small x), and the NNLO massive OMEs (large Q^2)

Impact of high twists on SLAC data

sa, Blümlein, Moch PRD 86, 054009 (2012)



Power-like terms affect comparison even with a “safe” cut $W^2 \geq 12.5 \text{ GeV}^2$

Checking styles of PDF shape

	ABMP16	CJ15	CT10	CT14	epWZ16	MMHT14
N_{PDF}	28	21	26	26	14	31
μ_0^2 (GeV ²)	9	1.69	1.69	1.69	1.9	1
χ^2	4065	4108	4148	4153	4336	4048
PDF shape	$x^\alpha(1-x)^\beta$ $\exp[P(x, \ln(x))]$	$x^\alpha(1-x)^\beta P(x, \sqrt{x})$	$x^\alpha(1-x)^\beta$ $\exp[P(x, \sqrt{x})]$	$x^\alpha(1-x)^\beta$ $\exp[P(x, \sqrt{x})]$	$x^\alpha(1-x)^\beta P(x, \sqrt{x})$	$x^\alpha(1-x)^\beta P(x, \sqrt{x})$
Constraints		$\bar{u}=\bar{d} \quad (x \rightarrow 0)$	$\alpha_{uv}=\alpha_{dv}$ $\alpha_{\bar{u}}=\alpha_{\bar{d}}=\alpha_s$ $\bar{u}=\bar{d} \quad (x \rightarrow 0)$	$\alpha_{uv}=\alpha_{dv}$ $\beta_{uv}=\beta_{dv}$ $\alpha_{\bar{u}}=\alpha_{\bar{d}}=\alpha_s$	$\alpha_{\bar{u}}=\alpha_{\bar{d}}=\alpha_s$ $\bar{u}=\bar{d} \quad (x \rightarrow 0)$	
$\alpha_s(M_Z)$	0.1153	0.1147	0.1150	0.1160	0.1162	0.1158

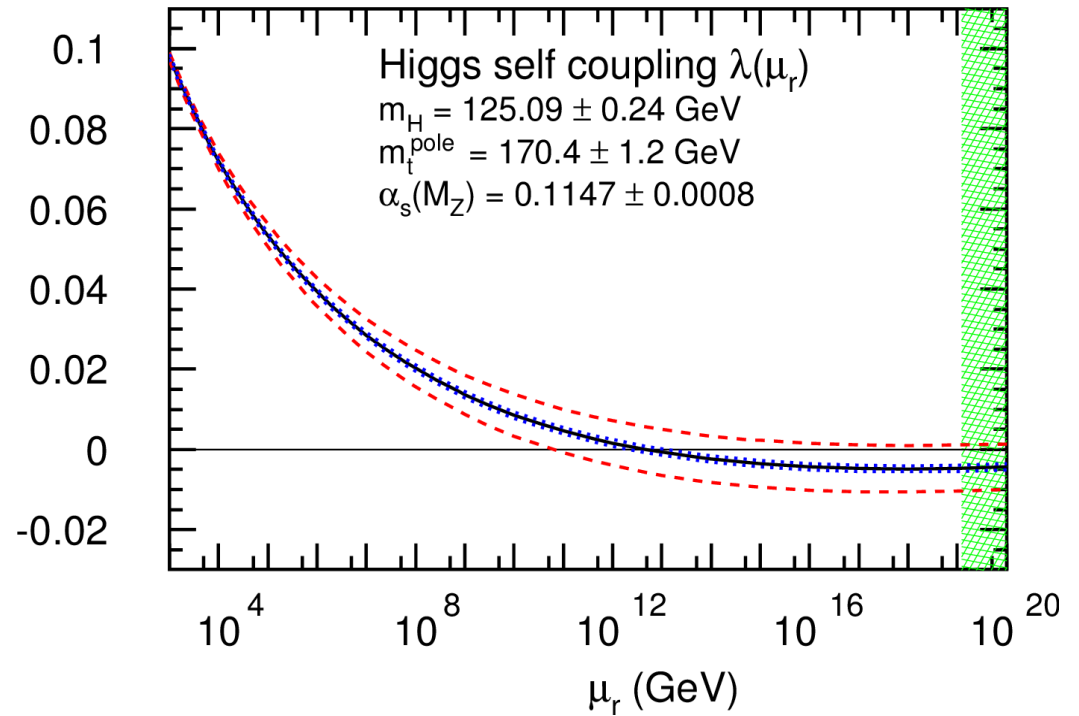
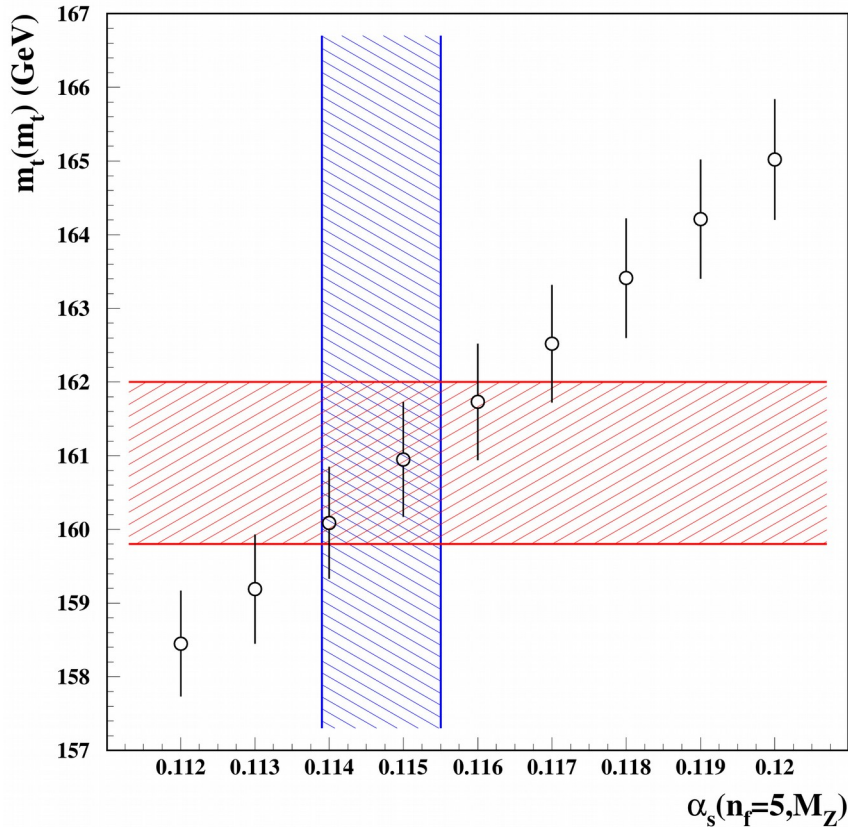
- Various PDF-shape modifications provide comparable description with $N_{\text{PDF}} \sim 30$
- Some deterioration, which happens in cases is apparently due to constraints on large(small)-x exponents

Conservative estimate of uncertainty in $\alpha_s(M_Z)$: 0.0007, more optimistic: 0.0003

Electroweak vacuum stability

$$m_H = 129.6 \text{ GeV} + 1.8 \times \left(\frac{m_t^{\text{pole}} - 173.34 \text{ GeV}}{0.9} \right) - 0.5 \times \left(\frac{\alpha_s^{(n_f=5)}(M_Z) - 0.1184}{0.0007} \right) \text{ GeV} \pm 0.3 \text{ GeV},$$

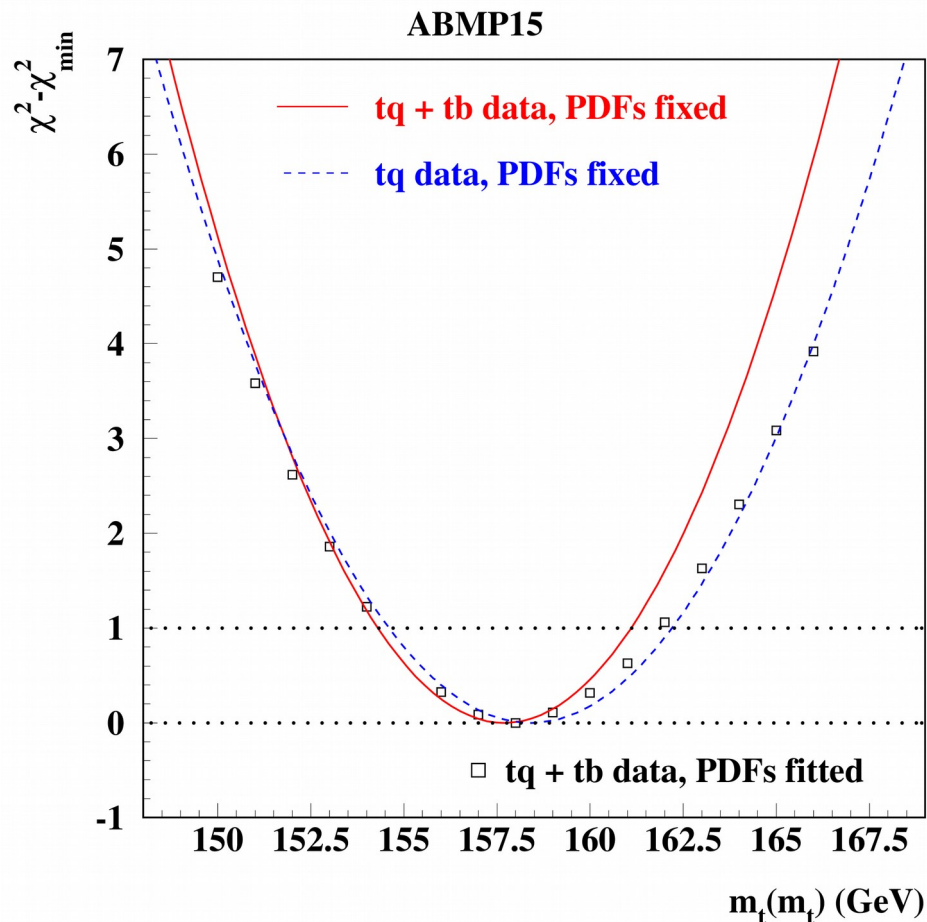
Buttazzo et al., JHEP 12, 089 (2013)



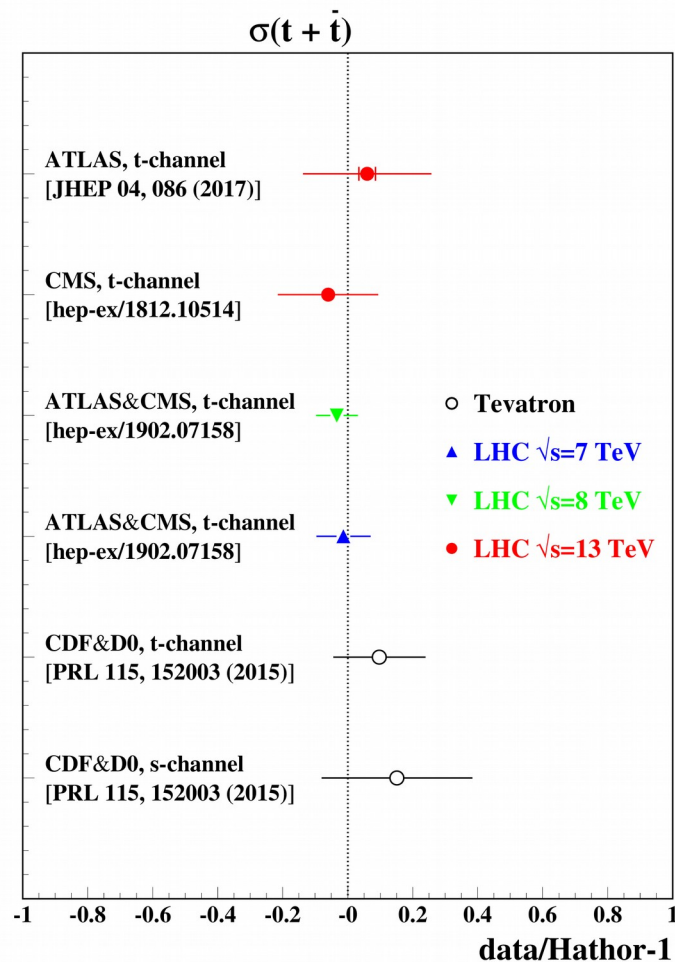
Mr: Kniehl, Pikelner, Veretin CPC 206, 84 (2016)

Vacuum stability is quite sensitive to the t -quark mass; stability is provided up to Planck-mass scale using α_s and m_t in a consistent way.

t-quark: single production (mass determination)



sa, Moch, Thier PLB 763, 341 (2016)



$m_t(m_t) = 161.1 \pm 3.8 \text{ GeV}$ (single-top only)

Channel	ABM12 [21]	ABMP15 [52]	CT14 [55]	MMHT14 [56]	NNPDF3.0 [57]
$t\bar{t}$	158.6 ± 0.6	158.4 ± 0.6	164.7 ± 0.6	164.6 ± 0.6	164.3 ± 0.6
t -channel	158.7 ± 3.7	158.0 ± 3.7	160.1 ± 3.8	160.5 ± 3.8	164.0 ± 3.8
s - & t -channel	158.4 ± 3.3	157.7 ± 3.3	159.1 ± 3.4	159.6 ± 3.4	162.4 ± 3.5